Available online at www.sciencedirect.com
ScienceDirect
Journal of the Mechanics and Physics of Solids
55 (2007) 1–34

JOURNAL OF THE MECHANICS AND PHYSICS OF SOLIDS

www.elsevier.com/locate/jmps

Structural interfaces in linear elasticity. Part I: Nonlocality and gradient approximations

K. Bertoldi, D. Bigoni*, W.J. Drugan[1]

Dipartimento di Ingegneria Meccanica e Strutturale, Università di Trento, Via Mesiano 77, I-38050 Trento, Italy

Received 9 February 2006; received in revised form 13 June 2006; accepted 15 June 2006

Abstract

Many biological and optimal materials, at multiple scales, consist of what can be idealized as continuous bodies joined by structural interfaces. Mechanical characterization of the microstructure defining the interface can nowadays be accurately done; however, such interfaces are usually analyzed employing models where those properties are overly simplified. To introduce into the analysis the microstructure properties, a new model of structural interfaces is proposed and developed: a true structure is introduced in the transition zone, joining continuous bodies, with geometrical and material properties directly obtained from those of the interfacial microstructure. First, the case of an elliptical inclusion connected by a structural interface to an infinite matrix is solved analytically, showing that nonlocal effects follow directly from the introduction of the structure, related to the inclination of the connecting elements. Second, starting from a discrete structure, a continuous model of a structural interface is derived. The usual zero-thickness linear interface model is shown to be a special case of this more general continuous structural interface model. Then, a gradient approximation of the interface constitutive law is rigorously derived: it is the first example of the analytical derivation of a nonlocal interface model from the microstructure properties. The effects introduced in the mechanical behavior by both the continuous model and its gradient approximation are illustrated by solving, for the first time, the problem of a circular

*Corresponding author. Tel.: +39 461882507; fax: +39 461882599.
E-mail addresses: katia.bertoldi@ing.unitn.it (K. Bertoldi), davide.bigoni@ing.unitn.it, bigoni@ing.unitn.it (D. Bigoni), drugan@engr.wisc.edu (W.J. Drugan).
URL: http://www.ing.unitn.it/~bigoni/.
[1]Permanent address: Department of Engineering Physics, University of Wisconsin-Madison, 1500 Engineering Drive, Madison, WI 53706, USA.

0022-5096/$ - see front matter
doi:10.1016/j.jmps.2006.06.004

inclusion connected to an infinite matrix by a structural interface and subject to remote uniform stress.

Keywords: Mechanical interfaces; Elliptical inclusions; Structural interfaces; Gradient models; Nonlocal effects

1. Introduction

There are many mechanical problems involving interfaces joining different parts of a continuous body. These transition zones are often characterized by well-defined microstructures: in Pinctada nacre, fibrils of organic matrix bridge the platelet lamellae (detail (A) of Fig. 1); a truss-like structure made of glass fibers bridges a crack in a short glass-fiber-reinforced polypropylene (detail (B) of Fig. 1); craze fibrils bridge the two bulk polymer surfaces at a crack tip in polystyrene (detail (C) of Fig. 1); in the meninges surrounding the human brain, trabeculae connect the subarachnoid space with the pia mater (detail (D) of Fig. 1); in a palm petiole, the relatively dense vascular bundles are distributed throughout a 'web' of parenchyma cells (detail (E) of Fig. 1). Currently, the possibility to produce artificial material with this type of microstructure is being studied:

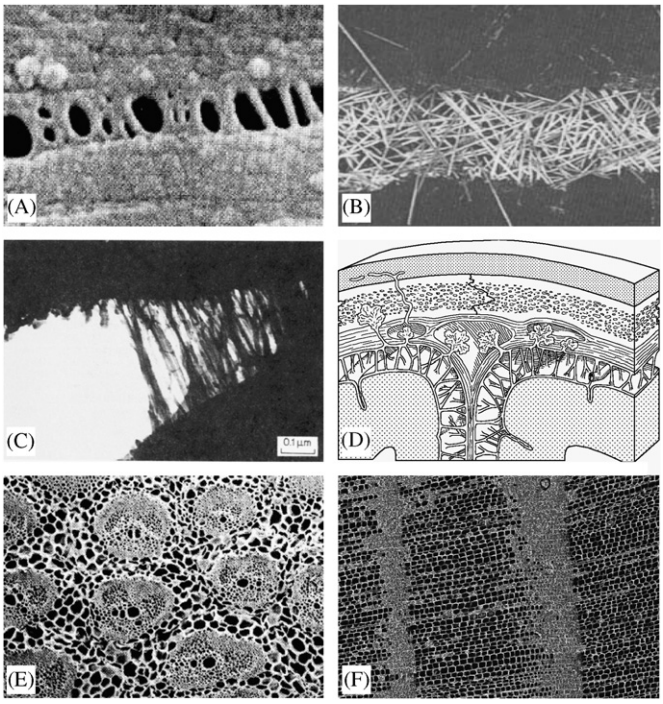

Fig. 1. Examples of structural interfaces in nature: (A) Pinctada nacre (figure from Jackson et al., 1988); (B) short glass-fiber-reinforced polypropylene (taken from Geers, 1997); (C) crack tip in polystyrene (taken from Xiao and Curtin, 1995); (D) meninges surrounding the human brain (adapted from Kahle and Frotscher, 2002); (E) cross-section of a palm (chamaerops humilis) petiole (taken from Gibson et al., 1995); (F) pyrolyzed wood infiltrated with Si (courtesy of Dr. L. Esposito, ISTEC CNR, Faenza, Italy).

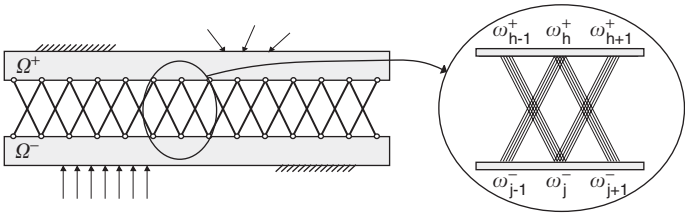

Fig. 2. A model of a structural interface.

for example, the process of ceramization of wood (Esposito et al., 2004) is employed to obtain porous components where the microstructure of the starting material is replicated in the ceramic component (detail (F) of Fig. 1). In solid mechanics, discrete structures joining continuous bodies can be found in cracks bridged by fibers (Rubinstein, 1994) and in the description of atomic interactions in both contact and fracture mechanics (Movchan et al., 2003; Gao et al., 2001).

Usually, mechanical interfaces are analyzed by employing the concept of a *zero-thickness imperfect interface*, based on the transmission conditions

$$[\![\boldsymbol{\sigma}]\!]\mathbf{n} = \mathbf{0}, \quad \boldsymbol{\sigma}^+\mathbf{n} = \mathbf{g}([\![\mathbf{u}]\!]), \tag{1}$$

where $\mathbf{n}$ is the unit vector normal to the interface, $\boldsymbol{\sigma}$ is the stress tensor, $\mathbf{u}$ is the displacement vector, $\boldsymbol{\sigma}^+$ is the stress on one side of the interface, $\mathbf{g}$ denotes a vectorial function of the displacement jump, and $[\![\cdot]\!]$ denotes the jump operator, defined as

$$[\![f]\!] = f^+ - f^-, \tag{2}$$

in which $+$ and $-$ denote the two sides of the interface. When the function $\mathbf{g}$ is linear and positive-definite, the formulation greatly simplifies, but it then allows unphysical interpenetration of the material in contact (when the interface is subject to compressive tractions). Interfacial nonlinearity may be introduced to model different situations of interest [see, for instance, applications in: fragmentation and decohesion (Camacho and Ortiz, 1996; Needleman, 1992; Rice and Wang, 1989), interactions between inclusions (Levy and Hardikar, 1999), bifurcation (Radi et al., 1999), composites (Levy and Dong, 1998; Lipton and Talbot, 2001), biomechanics (Mann et al., 1997; Gei et al., 2002)] and may avoid the interpenetration by the introduction of a suitable penalty in compression. Recently, efforts have been made to provide models of thick interfaces, where the boundary value problem consisting of a three-phase configuration is replaced by a problem which involves only two phases plus some matching condition simulating the interphase (Benveniste and Miloh, 2001; Hashin, 2002; Rubin and Benveniste, 2004).

Mechanical interfaces are characterized by a finite thickness and structural properties, which are often overly simplified by the above model, Eqs. (1). To provide more realistic models of thick interfaces, Bigoni and Movchan (2002) have suggested modelling the interface as a truly discrete structure. In particular, they introduced the concept of a structural interface which possesses a finite width and specific mechanical properties (see the sketch in Fig. 2, specialized to two-dimensional deformations for simplicity). Not only does this permit capturing the precise structure of the actual interface, the incorporation of a specific structure in general introduces *nonlocal effects*, and these follow from the model

in a natural and rational way.[2] In other words, while *a zero-thickness interface model is phenomenological*, a structural interface provides a direct description of the relevant microstructure. The model proposed by Bigoni and Movchan (called 'BM-model' in the following[3]) defines a quasi-local interface in the sense that nonlocality is confined to the joining of opposite points on the interface. The BM-model is generalized in the present paper to incorporate the full nonlocality induced by a generic truss structure joining two continuous media, in general not at directly neighboring locations. For simplicity, the continuous media are modelled as homogeneous, isotropic, linear elastic materials and loaded on their boundaries (Fig. 2). In this discrete/continuum problem, a difficulty arises in describing the contact between the structure and the elastic media. This is overcome by working with mean values of displacements and tractions at the joints and assuming that the joints are characterized by a given, small dimension. Following this approach, the problem can be analytically[4] tackled.

The paper is organized as follows. The governing equations for a structural interface are introduced in Section 2. In Section 3, the problem of an elliptical inclusion connected by a structural interface to an infinite medium loaded by a uniform remote stress is analyzed. It is shown that this case can be solved analytically, and it permits us to systematically investigate the effects of the interfacial nonlocality. Starting from a discrete structure, a continuous model of a structural interface and its gradient approximation are rigorously derived in Section 4, thus providing the first example of analytical derivation of a gradient model. The particular case of a circular inclusion is analytically solved both with the structural interface and with its gradient approximation, allowing a rigorous comparison between the two models. These solutions represent the first two-dimensional closed-form solutions to a problem involving a nonlocal interface.

The solution of the problem of an elliptical inclusion in an infinite elastic matrix permits analysis of possible neutrality (the inclusion does not perturb the ambient field) and of the effective properties of dilute composites containing inclusions having structural interfaces. Treatment of these problems is deferred to Part II of this article.

2. Governing equations for a structural interface

Two elastic continuous bodies connected by a structural interface represent a model of a *multistructure*, namely, an elastic multidimensional body. These types of structure are very common in many fields of engineering and have recently received much attention (Ciarlet et al., 1989; Ciarlet, 1990, 1997; Puel and Zuazua, 1993; Argatov and Nazarov, 1994; Conca and Zuazua, 1994; Kozlov et al., 1999, 2001).

[2]Zero-thickness nonlocal interfaces could obviously be introduced, but the nonlocality would enter the formulation in a purely phenomenological way.

[3]The 'smeared BM-model' will denote the thick interface characterized by constitutive equations (10) and (11) of Bigoni and Movchan (2002) with null shearing stiffness, $s_\theta = 0$, whereas 'discrete BM-model' will indicate a thick interface with purely radial bars.

[4]The proposed approach can be easily implemented via a boundary element technique, which has been used to check all analytical solutions presented in this paper. The numerical technique will be presented elsewhere.

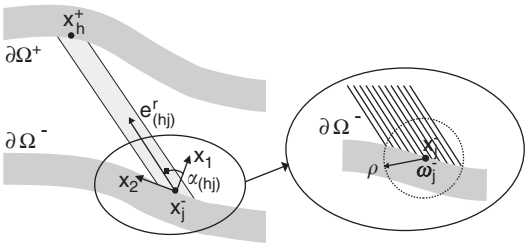

Fig. 3. Two elastic bodies connected by a filamentary structure.

Inspired by the above formulations, a simple model for the analysis of two-dimensional multistructures is developed below.[5] This is based on the following assumptions.

- *Solid/structure junctions*: As illustrated in Fig. 3, let us denote by Ω^- and Ω^+ (with boundary $\partial\Omega^-$ and $\partial\Omega^+$, respectively) the two continuous linear elastic two-dimensional bodies connected by the structural interface. The jth junction between a bar and the continuous body is represented by a contact region $\boldsymbol{\omega}_j^\pm$ on $\partial\Omega^\pm$,

$$\boldsymbol{\omega}_j^\pm = \partial\Omega^\pm \cap B(\mathbf{x}_j^\pm, \rho), \tag{3}$$

where $B(\mathbf{x}_j^\pm, \rho)$ is the disk of radius ρ centered at $\mathbf{x}_j^\pm$ and $\pm$ stands for either $+$ or $-$. In addition, it is assumed that $\partial\Omega^\pm$ possesses continuous curvature near $\mathbf{x}_j^\pm$, so that there exists a class $\mathscr{C}^2$ function

$$\mathbf{v}_j^\pm : [-\ell_j, \ell_j] \to \boldsymbol{\omega}_j^\pm, \quad \mathbf{x}^\pm = \mathbf{v}_j^\pm(\ell), \tag{4}$$

mapping the segment $[-\ell_j, \ell_j]$ into the contact region $\boldsymbol{\omega}_j^\pm$ and transforming $\ell = 0$ into the point $\mathbf{x}_j^\pm$, so that

$$\mathbf{x}_j^\pm = \mathbf{v}_j^\pm(0). \tag{5}$$

At the junction, the load is transmitted as if the bar were a 'linear, filamentary structure' connecting the junctions of central points $\mathbf{x}_h^+$ and $\mathbf{x}_j^-$, defined by the direction specified by the unit vector $\mathbf{e}_{(hj)}^r$, with components $\{\cos\alpha_{(hj)}, \sin\alpha_{(hj)}\}$, where $\alpha_{(hj)}$ denotes the angle between the filament hj and the x_1-axis of an arbitrary reference system. In addition, we introduce for later use the function $l(\alpha_{(hj)})$, so that points on the opposite sides of the interface connected by a bar are related via

$$\mathbf{x}_h^+ = \mathbf{x}_j^- + l(\alpha_{(hj)})\mathbf{e}_{(hj)}^r. \tag{6}$$

The traction $\mathbf{t}^h$ transmitted at the h-junction is assumed to be a linear function of the bar elongation, so that

$$\mathbf{t}^j(\mathbf{x}^-) = k_{(hj)}[(\mathbf{u}(\mathbf{x}^+) - \mathbf{u}(\mathbf{x}^-)) \cdot \mathbf{e}_{(hj)}^r]\mathbf{e}_{(hj)}^r, \quad \mathbf{x}^+ \in \boldsymbol{\omega}_h^+, \ \mathbf{x}^- \in \boldsymbol{\omega}_j^-, \tag{7}$$

[5] This will be explained assuming for simplicity that the rods of the truss structure describing the interface connect the two solids directly. The extension to the situation in which there are intermediate nodes in the structure is straightforward.

where $k_{(hj)}$ is the stiffness coefficient of the filament connecting points $\mathbf{x}^+$ and $\mathbf{x}^-$. In addition, the equilibrium of the filament hj requires that

$$\mathbf{t}^h(\mathbf{x}^+) = -\mathbf{t}^j(\mathbf{x}^-), \quad \mathbf{x}^+ \in \boldsymbol{\omega}_h^+, \ \ \mathbf{x}^- \in \boldsymbol{\omega}_j^-. \tag{8}$$

Since in a junction M different bars can converge, each characterized by a stiffness $k_{(hj)}$ and inclination $\alpha_{(hj)}$, Eq. (7) is replaced by

$$\mathbf{t}^j(\mathbf{x}^-) = \sum_{h=1}^{M} k_{(hj)}[(\mathbf{u}(\mathbf{x}^+) - \mathbf{u}(\mathbf{x}^-)) \cdot \mathbf{e}^r_{(hj)}]\mathbf{e}^r_{(hj)}, \quad \mathbf{x}^+ \in \boldsymbol{\omega}_h^+, \ \ \mathbf{x}^- \in \boldsymbol{\omega}_j^-. \tag{9}$$

- *The boundary value problem*: The stress field $\boldsymbol{\sigma}$ in the continuous elastic bodies (in the absence of body forces) satisfies

$$\begin{cases} \operatorname{div}\boldsymbol{\sigma}(\mathbf{x}) = \mathbf{0}, & \mathbf{x} \in \Omega^{\pm}, \\ \boldsymbol{\sigma}(\mathbf{x}^+)\mathbf{n}(\mathbf{x}^+) = \displaystyle\sum_{j=1}^{M} k_{(hj)}[(\mathbf{u}(\mathbf{x}^+) - \mathbf{u}(\mathbf{x}^-)) \cdot \mathbf{e}^r_{(hj)}]\mathbf{e}^r_{(jh)}, & \mathbf{x}^+ \in \boldsymbol{\omega}_h^+, \mathbf{x}^- \in \boldsymbol{\omega}_j^-, \\ \boldsymbol{\sigma}(\mathbf{x}^-)\mathbf{n}(\mathbf{x}^-) = \displaystyle\sum_{h=1}^{M} k_{(hj)}[(\mathbf{u}(\mathbf{x}^+) - \mathbf{u}(\mathbf{x}^-)) \cdot \mathbf{e}^r_{(hj)}]\mathbf{e}^r_{(hj)}, & \mathbf{x}^+ \in \boldsymbol{\omega}_h^+, \mathbf{x}^- \in \boldsymbol{\omega}_j^-, \\ \text{prescribed tractions or displacements on } \partial\Omega^{\pm} \Big\backslash \left(\displaystyle\bigcup_{q=1}^{N} \boldsymbol{\omega}_q^{\pm} \right), \end{cases} \tag{10}$$

where $\mathbf{n}$ is the outward unit normal to the boundary of the two connected bodies and q is an integer ranging between 1 and the number of junctions N, possibly taking different values on $\partial\Omega^+$ and $\partial\Omega^-$. Note that the displacements, and therefore the tractions transmitted by the interfacial structure to the continuous bodies at the junctions, have an initially unknown distribution.

- *Problem formulation in terms of averaged tractions and displacements at the junctions*: A simplification of problem (10) is pursued here by working with averaged quantities at the junctions between bars and bodies. To this purpose, we introduce the averaged tractions and displacements at junctions as (here the superscript $\pm$ is omitted for conciseness)

$$\begin{aligned} \overline{\mathbf{t}}_j &= \frac{1}{|\boldsymbol{\omega}_j|}\int_{\boldsymbol{\omega}_j} \mathbf{t}(\mathbf{x}) = \frac{1}{|\boldsymbol{\omega}_j|}\int_{-\ell_j}^{\ell_j} \mathbf{t}(\mathbf{v}_j(\ell))|\mathbf{v}_j'(\ell)|\,\mathrm{d}\ell, \\ \overline{\mathbf{u}}_j &= \frac{1}{|\boldsymbol{\omega}_j|}\int_{\boldsymbol{\omega}_j} \mathbf{u}(\mathbf{x}) = \frac{1}{|\boldsymbol{\omega}_j|}\int_{-\ell_j}^{\ell_j} \mathbf{u}(\mathbf{v}_j(\ell))|\mathbf{v}_j'(\ell)|\,\mathrm{d}\ell, \end{aligned} \tag{11}$$

so that the boundary value problem (10) is replaced by

$$\begin{cases} \operatorname{div}\boldsymbol{\sigma}(\mathbf{x}) = \mathbf{0}, & \mathbf{x} \in \Omega^{\pm}, \\ \boldsymbol{\sigma}(\mathbf{x}^+)\mathbf{n}(\mathbf{x}^+) = \displaystyle\sum_{j=1}^{M} k_{(hj)}[(\overline{\mathbf{u}}_h^+ - \overline{\mathbf{u}}_j^-) \cdot \mathbf{e}^r_{(hj)}]\mathbf{e}^r_{(jh)}, & \mathbf{x}^+ \in \boldsymbol{\omega}_h^+, \\ \boldsymbol{\sigma}(\mathbf{x}^-)\mathbf{n}(\mathbf{x}^-) = \displaystyle\sum_{h=1}^{M} k_{(hj)}[(\overline{\mathbf{u}}_h^+ - \overline{\mathbf{u}}_j^-) \cdot \mathbf{e}^r_{(hj)}]\mathbf{e}^r_{(hj)}, & \mathbf{x}^- \in \boldsymbol{\omega}_h^-, \\ \text{prescribed tractions or displacements on } \partial\Omega^{\pm} \Big\backslash \left(\displaystyle\bigcup_{q=1}^{N} \boldsymbol{\omega}_q^{\pm} \right), \end{cases} \tag{12}$$

where the initially unknown traction distributions over the junctions is replaced by a uniform distribution. Since we will replace the solution of problem (10) by the solution of the simpler problem (12), a digression is now needed to comment on the difference between the two solutions. In particular, we assume that the size of the junction zones is small when compared to the dimension of the connected bodies, so that these zones 'contract' onto the points $\mathbf{x}_j$. It can then be shown (Appendix A) by employing results due to Mises (1945), Sternberg (1954) and Gurtin (1972) that the elastic energy evaluated by solving (10) differs from that evaluated by solving (12) by terms $O(\ell_j^2)$.

Problem (12) is employed as the basis for analyzing structural interfaces. We proceed as follows:

- The solutions in the jointed bodies $\Omega^{\pm}$ for uniform traction distributions over the junction regions $\boldsymbol{\omega}_h$ is constructed, so that the displacements at the junction points $\mathbf{u}(\mathbf{x}_h)$ are written as functions of the (for the moment unknown) uniform tractions $\mathbf{t}(\mathbf{x}_h)$ applied at joint regions and of the prescribed 'external' boundary conditions.
- The conditions of equilibrium of all the nodes of the truss structure defining the interface are imposed. To this purpose, Eq. $(12)_2$ is employed to enforce equilibrium for the nodes located at the junctions with the solid bodies, whereas for nodes internal to the structure, equilibrium is imposed using classical methods of structural mechanics. All tractions at junctions and normal stresses within the bars are obtained in this way.

3. Analytical solution for an elliptical inclusion connected by a structural interface to an infinite medium

In order to apply the methodology described in Section 2 to the problem of an elliptical elastic inclusion connected by a structural interface to an infinite elastic sheet, we need some preliminary results. These are the three solutions corresponding to

- a self-equilibrated but otherwise arbitrary distribution of uniform loadings acting on separated portions of an elliptical elastic disk;
- a self-equilibrated but otherwise arbitrary distribution of uniform loadings acting on separated portions of an elliptical hole in an infinite elastic sheet;
- an elliptical hole in an infinite elastic sheet, loaded by a remote uniform stress.

The solution to the third problem above is well known and can be found in Muskhelishvili (1953), whereas we were unable to find solutions of the first two problems in the literature. Therefore, we have solved the first two problems in Appendices B and C by employing the Kolossoff–Muskhelishvili (1953) complex potentials $\phi(z)$ and $\psi(z)$. In terms of these potentials, the general solution to plane equilibrium problems for homogeneous, isotropic linear elastic materials can be expressed in polar components as

$$\begin{aligned} &2\mu(u_r + \mathrm{i}u_\theta) = \mathrm{e}^{-\mathrm{i}\theta}[\kappa\phi(z) - z\overline{\phi'(z)} - \overline{\psi(z)}],\\ &\sigma_{rr} + \sigma_{\theta\theta} = 4\mathrm{Re}[\phi'(z)],\\ &\sigma_{\theta\theta} - \sigma_{rr} + 2\mathrm{i}\sigma_{r\theta} = 2\mathrm{e}^{2\mathrm{i}\theta}[\bar{z}\phi''(z) + \psi'(z)], \end{aligned} \tag{13}$$

where $z = x_1 + ix_2 = re^{i\theta}$, prime denotes derivative with respect to a function's argument, overbar denotes complex conjugate, $\kappa = 3 - 4\nu$ for plane strain and $\kappa = (3 - \nu)/(1 + \nu)$ for plane stress, and μ and ν are the shear modulus and the Poisson ratio, respectively. When tractions $\tilde{\mathbf{t}}$ are prescribed on the boundary, the boundary condition can be written as

$$\phi(z) + z\overline{\phi'(z)} + \overline{\psi(z)} = f_1 + if_2, \tag{14}$$

where, for s denoting arc length along the boundary,

$$f_1 + if_2 = i\int_s [\tilde{t}_1(s) + i\tilde{t}_2(s)]\,ds. \tag{15}$$

Let us consider the complex plane z where the elliptical inclusion is represented by an ellipse of semi-axes a and b. It is well known that the function $\omega(\zeta)$, that conformally maps the region interior to an ellipse into a disk, is very complicated. Following Muskhelishvili (1953) it is expedient to introduce the analytic function

$$z = \omega(\zeta) = R\left(\zeta + \frac{m}{\zeta}\right), \tag{16}$$

where

$$R = \frac{a+b}{2}, \quad m = \frac{a-b}{a+b}. \tag{17}$$

This function conformally maps the region corresponding to an elliptical inclusion in the z-plane slit along the major axis of the ellipse between $\pm\sqrt{a^2 - b^2}$ to an annulus in the ζ-plane, having unit external radius and internal radius equal to $\sqrt{m}$. The actual physical problem of a loaded elliptical inclusion is obtained from this slit inclusion by enforcing continuity of the analytic functions across the slit (see Appendix B). Note that $0 \leqslant m \leqslant 1$ and the limiting values 0 and 1 correspond to a circular and a line inclusion, respectively. The same function (16) maps the region external to the ellipse into the region external to the unit circle.

Employing the conformal mapping (16) and taking for ζ the polar form

$$\zeta = \rho e^{i\beta}, \tag{18}$$

Eqs. (13)–(14) give

- The displacement components

$$2\mu|\omega'(\zeta)|(u_r + iu_\theta) = \frac{\overline{\zeta}}{\rho}\overline{\omega'(\zeta)}\left[k\phi(\zeta) - \frac{\omega(\zeta)}{\overline{\omega'(\zeta)}}\overline{\phi'(\zeta)} - \overline{\psi(\zeta)}\right]. \tag{19}$$

- The stress components

$$\begin{aligned}
&\sigma_{rr} + \sigma_{\theta\theta} = 4\,\mathrm{Re}[\Phi(\zeta)],\\
&\sigma_{\theta\theta} - \sigma_{rr} + i2\sigma_{r\theta} = \frac{2\zeta^2}{\rho^2\overline{\omega'(\zeta)}}[\overline{\omega(\zeta)}\Phi'(\zeta) + \omega'(\zeta)\Psi(\zeta)],
\end{aligned} \tag{20}$$

where

$$\Phi(\zeta)=\frac{\phi'(\zeta)}{\omega'(\zeta)},\quad \Psi(\zeta)=\frac{\psi'(\zeta)}{\omega'(\zeta)}. \tag{21}$$

- The boundary conditions

$$\phi(\sigma)+\frac{\omega(\sigma)}{\overline{\omega'(\sigma)}}\overline{\phi'(\sigma)}+\overline{\psi(\sigma)}=F(\sigma), \tag{22}$$

where $\sigma=e^{i\beta}$ denotes a point on the unit circle $\rho=1$ and $F(\sigma)$ is determined at the boundary of the unit circle from the known values f_1+if_2 specified in the z-plane on the boundary of the ellipse, Eq. (15).

3.1. Solution for an elliptical inclusion subject to uniform loadings distributed over portions of its boundary

An elliptical inclusion is considered, with N uniform tractions having normal and tangential components p_k and s_k, respectively, acting on the portion $z_k^- z_k^+$ of its boundary, see Fig. 4. The resultant of all the loads acting on the inclusion is assumed to be zero. Since the complex functions $\phi(\zeta)$ and $\psi(\zeta)$, representing the solution of the problem, are holomorphic in the circular ring limited by the radii $\rho_{\text{ext}}=1$ and $\rho_{\text{int}}=\sqrt{m}$, they can be represented as Laurent series

$$\phi(\zeta)=\sum_{k=-\infty}^{+\infty}a_k\zeta^k,\quad \left(1-\frac{1}{\zeta^2}\right)\psi(\zeta)=\sum_{k=-\infty}^{+\infty}b_k\zeta^k. \tag{23}$$

The complete derivation of the coefficients a_k and b_k appearing in Eq. (23) is given in Appendix B yielding

$$\begin{cases} a_1=\dfrac{\bar{A}_1-m\bar{A}_{-1}}{2(1-m^2)},\\ a_k=\dfrac{kc_k(m-m^{-1})-\bar{c}_k(m^k-m^{-k})}{k^2(m-m^{-1})^2-(m^k-m^{-k})^2},\quad k>1,\\ b_k=\bar{A}_{-k}-m\bar{A}_{-k-2}-m^k\bar{a}_k+m^{k+3}\bar{a}_{k+2}-(k+2)a_{k+2}-mka_k, \end{cases} \tag{24}$$

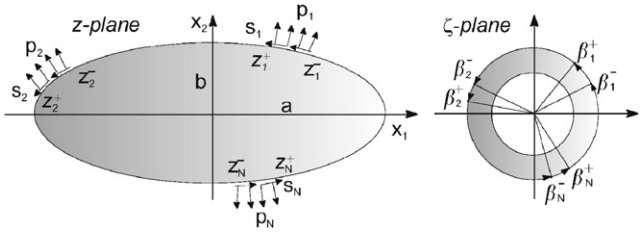

Fig. 4. Elliptical inclusion with N applied uniform normal and tangential traction distributions in the z-plane, and its conformal mapping in the ζ-plane. The slit is not shown in the z-plane, since it is eliminated in the solution procedure by enforcing continuity of the solution across it.

where

$$c_k = \bar{A}_{-k} - \frac{\bar{A}_k}{m^k} \tag{25}$$

and

$$A_k = \frac{1}{2\pi}\sum_{w=1}^{N}(p_w + \mathrm{i}s_w)\left\{\frac{\mathrm{i}}{k}(z_w^- \mathrm{e}^{-\mathrm{i}k\beta_w^-} - z_w^+ \mathrm{e}^{-\mathrm{i}k\beta_w^+}) + \frac{\mathrm{e}^{-\mathrm{i}k\beta_w^+}}{k^2-1}[\mathrm{i}(b+ak)\cos\beta_w^+ - (a+bk)\sin\beta_w^+] - \frac{\mathrm{e}^{-\mathrm{i}k\beta_w^-}}{k^2-1}[\mathrm{i}(b+ak)\cos\beta_w^- - (a+bk)\sin\beta_w^-]\right\}. \tag{26}$$

When the inclusion is circular, so that $m = 0$, and loaded by an arbitrary number of distributed, uniform tractions, the solution has a closed form given by

$$\begin{aligned}\phi(\zeta) = & -\frac{R}{4\pi}\sum_{k=1}^{N}(p_k + \mathrm{i}s_k)[\zeta(\beta_k^- - \beta_k^+) + 2\mathrm{i}(\mathrm{e}^{\mathrm{i}\beta_k^-} - \zeta)\log(1 - \mathrm{e}^{-\mathrm{i}\beta_k^-}\zeta) \\ & - 2\mathrm{i}(\mathrm{e}^{\mathrm{i}\beta_k^+} - \zeta)\log(1 - \mathrm{e}^{-\mathrm{i}\beta_k^+}\zeta)], \\ \psi(\zeta) = & \frac{R}{2\pi\zeta}\sum_{k=1}^{N}\{2s_k\zeta(\mathrm{e}^{-\mathrm{i}\beta_k^-} - \mathrm{e}^{-\mathrm{i}\beta_k^+}) + [2s_k - (\mathrm{i}p_k + s_k)\mathrm{e}^{-\mathrm{i}\beta_k^-}\zeta] \\ & \times \log(1 - \mathrm{e}^{-\mathrm{i}\beta_k^-}\zeta) - [2s_k - (\mathrm{i}p_k + s_k)\mathrm{e}^{-\mathrm{i}\beta_k^+}\zeta]\log(1 - \mathrm{e}^{-\mathrm{i}\beta_k^+}\zeta)\}.\end{aligned} \tag{27}$$

In the limiting case of applied concentrated forces, obtained by letting the arc $\overset{\frown}{z_k^- z_k^+}$ tend to zero while increasing the magnitude of the load in such a way that

$$(p_k + \mathrm{i}s_k)|z_k^+ - z_k^-| \to P_k + \mathrm{i}S_k \tag{28}$$

remains a finite quantity, Eq. (26) reduces to

$$A_k = \frac{1}{2\pi k}\sum_{w=1}^{N}(P_w + \mathrm{i}S_w)\mathrm{e}^{\mathrm{i}(\theta_w^{\mathbf{n}} - k\beta_w)}, \tag{29}$$

where $\theta_w^{\mathbf{n}}$ denotes the angle between the unit outward normal and the x_1-axis at z_w.

The limiting case of a circular disk subjected to a self-equilibrated but otherwise arbitrary system of concentrated forces can be obtained from Eq. (27) as

$$\begin{aligned}\phi(\zeta) = & -\frac{1}{2\pi}\sum_{k=1}^{N}[(P_k + \mathrm{i}S_k)\mathrm{e}^{\mathrm{i}\beta_k}\log(1 - \mathrm{e}^{-\mathrm{i}\beta_k}\zeta)] - \frac{\zeta}{4\pi}\sum_{k=1}^{N}(P_k + \mathrm{i}S_k), \\ \psi(\zeta) = & \frac{1}{2\pi}\sum_{k=1}^{N}[(P_k - \mathrm{i}S_k)\mathrm{e}^{-\mathrm{i}\beta_k}\log(1 - \mathrm{e}^{-\mathrm{i}\beta_k}\zeta)] - \frac{1}{2\pi}\sum_{k=1}^{N}\frac{P_k + \mathrm{i}S_k}{\mathrm{e}^{\mathrm{i}\beta_k} - \zeta}.\end{aligned} \tag{30}$$

Muskhelishvili (1953) derived the solution for this particular case; Eqs. (30) are identical with his results.

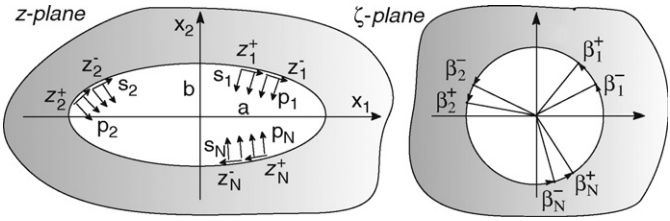

Fig. 5. Elliptical hole in an infinite elastic matrix with N applied uniform normal and tangential traction distributions in the z-plane, and its conformal mapping in the ζ-plane.

3.2. Solution for an elliptical hole in an infinite matrix subject to uniform loadings distributed over portions of the hole boundary

Here, we consider an infinite matrix containing an elliptical hole on which N piecewise uniform traction distributions having normal and tangential components p_k and s_k act on the parts $z_k^- z_k^+$, see Fig. 5, and whose total resultant vanishes. The solution that is obtained (derived in Appendix C) is a generalization of the case of an elliptical hole loaded by a pressure on a part of the boundary treated by Muskhelishvili (1953) and reduces to his solution in that special case; it is

$$\begin{aligned}
\phi(\zeta) = & -\frac{1}{2\pi \mathrm{i}}\sum_{k=1}^{N}(p_k+\mathrm{i}s_k)\Bigg\{R\Bigg[\sigma_k^+-\sigma_k^- -\frac{m}{\zeta}\log\frac{\sigma_k^+}{\sigma_k^-}+\left(\zeta+\frac{m}{\zeta}\right)\\
& \times\log\left(\frac{\sigma_k^+-\zeta}{\sigma_k^--\zeta}\right)\Bigg]+z_k^-\log(\sigma_k^--\zeta)-z_k^+\log(\sigma_k^+-\zeta)\Bigg\},\\
\psi(\zeta) = & -\frac{1}{2\pi \mathrm{i}}\sum_{k=1}^{N}(p_k-\mathrm{i}s_k)\Bigg\{R\Bigg[m\sigma_k^+-m\sigma_k^- -\frac{1}{\zeta}\log\frac{\sigma_k^+}{\sigma_k^-}+\left(m\zeta+\frac{1}{\zeta}\right)\\
& \times\log\left(\frac{\sigma_k^+-\zeta}{\sigma_k^--\zeta}\right)\Bigg]+\overline{z}_k^-\log(\sigma_k^--\zeta)-\overline{z}_k^+\log(\sigma_k^+-\zeta)\Bigg\}-\frac{\zeta(1+m\zeta^2)}{\zeta^2-m}\phi'(\zeta). \quad (31)
\end{aligned}$$

The limiting case of concentrated forces applied on the elliptical hole surface is obtained by the same procedure as in the case of the elliptical inclusion (see Eq. (28)), so that the solution for an elliptic hole subjected to N concentrated loads is obtained from Eq. (31) as

$$\begin{aligned}
\phi(\zeta) = & \frac{1}{2\pi}\sum_{k=1}^{N}(P_k+\mathrm{i}S_k)\mathrm{e}^{\mathrm{i}\theta_k^{\mathbf{n}}}\log(\sigma_k-\zeta),\\
\psi(\zeta) = & -\frac{1}{2\pi}\sum_{k=1}^{N}(P_k-\mathrm{i}S_k)\mathrm{e}^{-\mathrm{i}\theta_k^{\mathbf{n}}}\log(\sigma_k-\zeta)+\frac{1}{2\pi}\frac{\zeta(1+m\zeta^2)}{\zeta^2-m}\sum_{k=1}^{N}\frac{(P_k+\mathrm{i}S_k)\mathrm{e}^{\mathrm{i}\theta_k^{\mathbf{n}}}}{(\sigma_k-\zeta)}, \quad (32)
\end{aligned}$$

where $\theta_k^{\mathbf{n}}$ denotes the angle between the unit inward normal and the x_1-axis at z_k. The case of a circular hole in an infinite matrix is recovered simply by putting $m=0$ and $\theta_k^{\mathbf{n}}=\beta_k$ in Eqs. (31) and (32).

3.3. Solution for an elliptical hole in an infinite matrix subject to uniform stress at infinity

The case of an infinite elastic plane with a traction-free elliptical hole loaded at infinity by uniform stress of components $\sigma_{11}^{\infty}, \sigma_{12}^{\infty}, \sigma_{22}^{\infty}$ is well known. In this case the solution is given by

$$\phi(\zeta) = \Gamma_1 R\left(\zeta - \frac{m}{\zeta}\right) - \frac{\overline{\Gamma}_2 R}{\zeta},$$
$$\psi(\zeta) = \Gamma_2 R\zeta - \frac{\Gamma_1 R}{\zeta} - \frac{R}{\zeta(\zeta^2 - m)}[\overline{\Gamma}_2 + m\Gamma_1 + (\Gamma_1 + m\overline{\Gamma}_2 + 2m^2\Gamma_1)\zeta^2], \tag{33}$$

with

$$\Gamma_1 = \frac{\sigma_{11}^{\infty} + \sigma_{22}^{\infty}}{4}, \quad \Gamma_2 = \frac{\sigma_{22}^{\infty} - \sigma_{11}^{\infty}}{2} + \mathrm{i}\sigma_{12}^{\infty}. \tag{34}$$

3.4. Elliptical inclusion connected to an infinite matrix by a structural interface: results

As a first example, we consider an elliptical inclusion of minor (major) semi-axis b^- (a^-), connected to an infinite matrix with an elliptical hole of minor (major) semi-axis b^+ (a^+) by three different structures: the discrete BM-model, a Warren truss structure, and a hexagonal lattice structure (see Fig. 6). Besides the structure geometry and the remote applied stress, the solution depends on

$$\frac{\mu^-}{\mu^+}, \quad \nu^{\pm}, \quad m^{\pm}, \quad \frac{t_b}{a^+}, \quad N, \quad \Lambda,$$

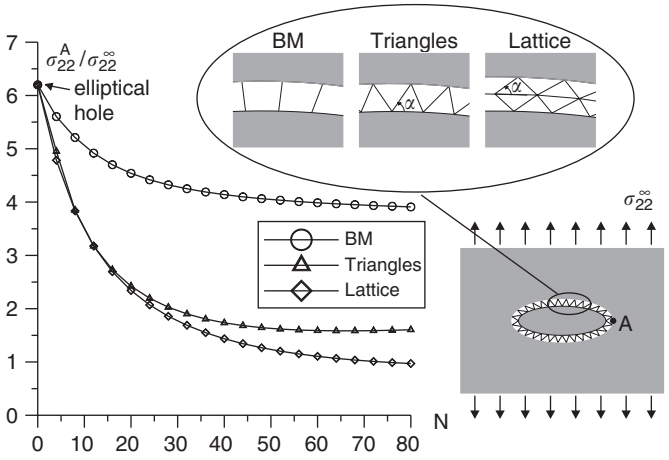

Fig. 6. Stress concentration (at point A) for an elliptical inclusion connected to the infinite matrix by a structural interface and loaded under uniaxial (vertical) stress, as a function of interfacial morphology and number N of bars. The inclusion is stiffer than the matrix ($\mu^-/\mu^+ = 10$) and $\nu^+ = \nu^- = \frac{1}{3}$, whereas the bars are characterized by $\Lambda = 0.075$ for the BM-model, $\Lambda = 0.075\,(2\sin^2\alpha)$ for the triangular structures and $\Lambda = 0.075\sin^2\alpha/(1+\cos^2\alpha)$ for the hexagonal lattice.

where + (−) denotes the matrix (inclusion) properties, t_b the bar thickness, N the number of bars, and the dimensionless parameter

$$\Lambda = \frac{2\mu^+}{(\kappa^+ + 1)kt_b} \tag{35}$$

describes the bar compliance as related to the matrix stiffness, so that $\Lambda = 0$ corresponds to a rigid bar, whereas $\Lambda = \infty$ to a bar with vanishingly small stiffness.

The two materials forming the inclusion and the matrix have properties $\mu^-/\mu^+ = 10$ and $v^+ = v^- = \frac{1}{3}$, whereas the elliptical inclusion and the elliptical hole in the matrix are characterized by $m^- = \frac{1}{2}$ and $m^+ = \frac{4}{9}$. A uniform uniaxial stress $\sigma_{22}^{\infty} = \mu^+/100$ is applied at infinity. The bars are characterized by $t_b/a^+ = 3/1000$ and $\Lambda = 0.075$ in the case of the BM-model, whereas $\Lambda = 0.075\ (2\sin^2\alpha)$ (with α shown in the detail of Fig. 6) for the triangular structures and $\Lambda = 0.075\sin^2\alpha/(1+\cos^2\alpha)$ for the hexagonal lattice, providing the same global stiffness in the radial direction. The largest stress concentration, namely, σ_{22} at point A, is plotted in Fig. 6 for different numbers of interfacial bars N ($2N$ in the

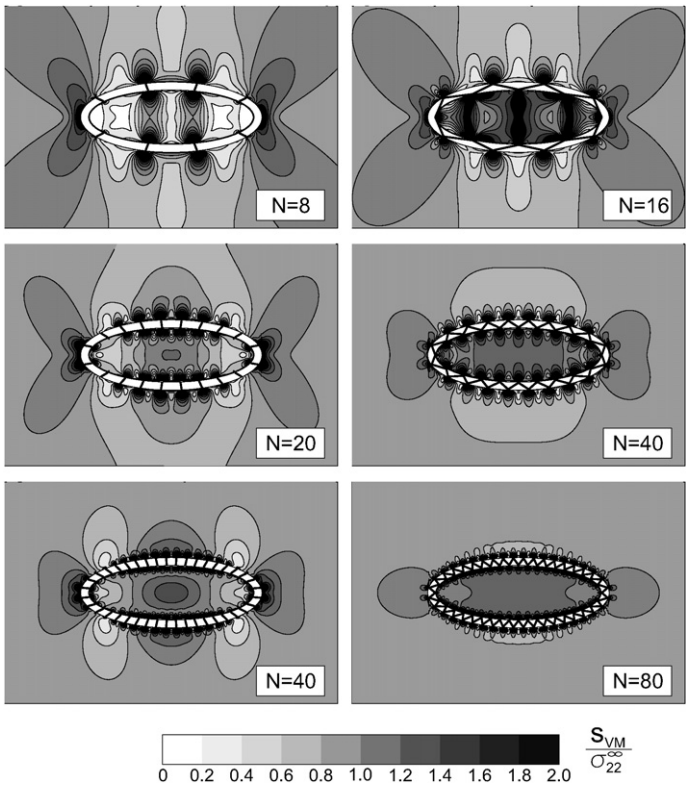

Fig. 7. von Mises stress distribution (normalized by remote stress) for a matrix connected by a structural interface to an elliptical inclusion, loaded by remote uniaxial (vertical) stress, as a function of interfacial morphology (discrete BM-model left, Warren truss structure right) and density of bars (number of bars increases from top to bottom). The inclusion is stiffer than the matrix ($\mu^-/\mu^+ = 10$) and $v^+ = v^- = \frac{1}{3}$, whereas the bars are characterized by $\Lambda = 0.075$ for the BM-model and $\Lambda = 0.075\,(2\sin^2\alpha)$ for the triangular structures.

case of triangles and $5N$ for lattice structures, but with the same global stiffness). It can be seen from the figure that the stress concentration is greater for the discrete BM-model than for the others, where the nonlocality introduced by the inclination of the bars decreases the severity of the stress field. For an elliptical hole the maximum stress concentration is given by the well-known formula

$$\frac{\sigma_{22}}{\sigma_{22}^{\infty}} = 1 + 2\frac{a}{b}, \tag{36}$$

so that in our case it is equal to 6.2, the value approached in the graphs when the number of bars approaches zero, while for an increasing number of bars, *the stress intensity tends to an asymptotic value that depends on the interface structure type*. Specifically, for high density of bars the stress concentration at point A tends to 3.9 in the case of the BM-model, 1.60 for the triangular structures, and 0.97 for the hexagonal lattice.

Since there is not much difference between results obtained employing the Warren truss structure and the hexagonal lattice, only the cases of the discrete BM-model and of the

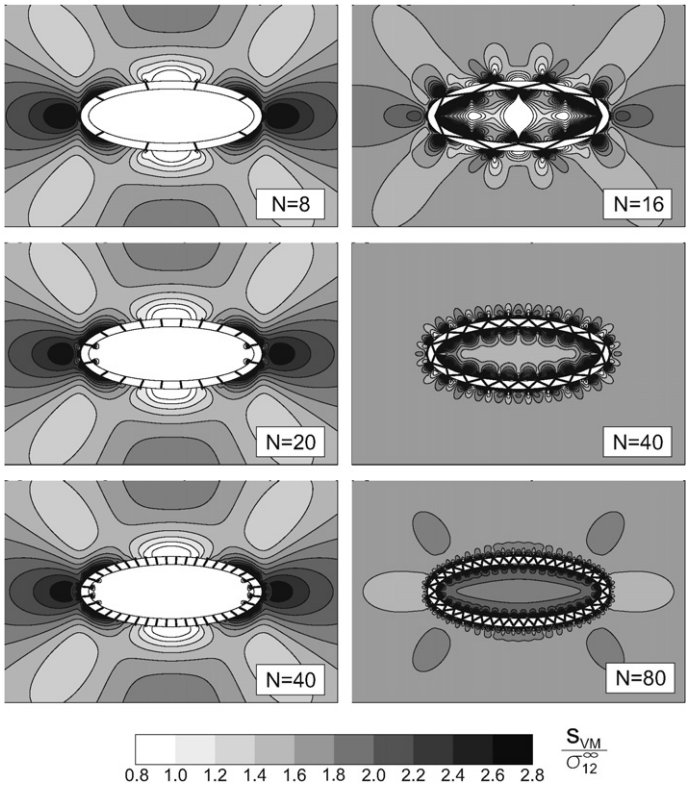

Fig. 8. von Mises stress distribution (normalized by remote stress) for a matrix connected by a structural interface to an elliptical inclusion, loaded by remote shear stress, as a function of interfacial morphology (discrete BM-model left, Warren truss structure right) and density of bars (number of bars increases from top to bottom). The inclusion is stiffer than the matrix ($\mu^-/\mu^+ = 10$) and $\nu^+ = \nu^- = \frac{1}{3}$, whereas the bars are characterized by $\Lambda = 0.075$ for the BM-model and $\Lambda = 0.075\,(2\sin^2\alpha)$ for the triangular structures.

Warren truss structure are considered in Figs. 7 and 8, where level sets of the von Mises stress, defined as

$$s_{\mathrm{VM}} = \sqrt{[(\sigma_1 - \sigma_2)^2 + (\sigma_1 - \sigma_3)^2 + (\sigma_3 - \sigma_2)^2]/2}, \tag{37}$$

with σ_i denoting the principal stresses, are plotted in a region near the inclusion (note that s_{VM} has been normalized by the remote stress). Fig. 7 corresponds to uniaxial vertical traction at infinity, while Fig. 8 corresponds to pure shear at infinity.

The figures show clearly the stress reduction caused by the interfacial structure, which becomes increasingly important as the density of the bars increases.

Note that for shear applied at infinity the inclusion remains almost unstressed when it is connected to the matrix by equally spaced single bars (the BM-model), Fig. 8 (left). In closure, we emphasize that all obtained results are analytical. Furthermore, they capture effects absent in all previous interface models: namely, the stress/deformation field effects due to a discrete-interface structure and the great stress concentration reduction due to the nonlocality that occurs as a direct consequence of the interface's discrete structure.

4. Continuous model and gradient approximation to structural interfaces

4.1. Continuous model for a double Warren truss structural interface—circular inclusion

Let us consider a circular inclusion of radius R connected to an infinite matrix by a double Warren truss structure of thickness δ, as shown in Fig. 9(B). We note that the angles α, β, and γ (see Fig. 9(A)) characterizing the interface are related as

$$\alpha = \beta + \gamma, \quad \beta = \arctan\frac{R\sin\gamma}{R + \delta - R\cos\gamma}, \quad \beta = \arcsin\left(\frac{R}{R+\delta}\sin\alpha\right). \tag{38}$$

For this particular geometry, the x_1-axis of the reference system drawn in Fig. 3 is chosen coincident with the outward normal of the inclusion (therefore identified with r, whereas the x_2 direction is identified by θ). Recalling from Eq. (6) that the two nodes $\mathbf{x}_h^+$ and $\mathbf{x}_j^-$ connected by the filament hj are related via the function $l(\alpha_{(hj)})$, for this particular case, the

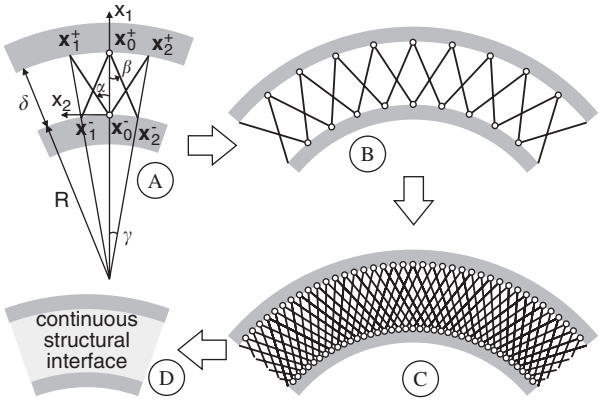

Fig. 9. Smearing of a double Warren truss structure into a continuous structural interface.

six points of the basis structural element shown in Fig. 9(A) can be easily described as

$$\begin{aligned} \mathbf{x}_1^+ &= \mathbf{x}_0^- + l(\alpha)\mathbf{e}^r(\alpha), \quad \mathbf{x}_2^+ = \mathbf{x}_0^- + l(\alpha)\mathbf{e}^r(-\alpha), \\ \mathbf{x}_1^- &= \mathbf{x}_0^+ - l(\alpha)\mathbf{e}^r(-\beta), \quad \mathbf{x}_2^- = \mathbf{x}_0^+ - l(\alpha)\mathbf{e}^r(\beta), \end{aligned} \tag{39}$$

where for the considered geometry, the function $l(\alpha)$ describing the hole as seen from the inclusion is given by

$$l(\alpha) = -R\cos\alpha + \sqrt{R^2\cos^2\alpha + 2R\delta + \delta^2}. \tag{40}$$

In addition, we observe that there is the following correspondence between the local and global coordinates of the six nodes of the basis structural element

$$\begin{aligned} &\mathbf{x}_0^- \to \{R, \theta\}, && \mathbf{x}_0^+ \to \{(R+\delta), \theta\}, \\ &\mathbf{x}_1^- \to \{R, (\theta+\gamma)\}, && \mathbf{x}_1^+ \to \{(R+\delta), (\theta+\gamma)\}, \\ &\mathbf{x}_2^- \to \{R, (\theta-\gamma)\}, && \mathbf{x}_2^+ \to \{(R+\delta), (\theta-\gamma)\}, \end{aligned} \tag{41}$$

where the angle γ is shown in Fig. 9(A). In order to develop a continuous model for the interface, one has:

- To consider a basic structural element, for instance, the truss element shown in Fig. 9(A).
- To combine the constitutive equation for each fiber meeting at a junction to get the structural behavior. For instance, for the geometry shown in Fig. 9(A), assuming that all filaments are characterized by the same stiffness k, we have

$$\begin{aligned} \mathbf{t}^-(\mathbf{x}_0^-) &= k[\Delta^+(\alpha)\mathbf{e}_r(\alpha) + \Delta^+(-\alpha)\mathbf{e}_r(-\alpha)], \\ \mathbf{t}^+(\mathbf{x}_0^+) &= -k[\Delta^-(\beta)\mathbf{e}^r(\beta) + \Delta^-(-\beta)\mathbf{e}^r(-\beta)], \end{aligned} \tag{42}$$

  where $\mathbf{t}^+$ and $\mathbf{t}^-$ are the tractions acting at the points $\mathbf{x}_0^+$ and $\mathbf{x}_0^-$ of the junctions, and we have defined

$$\begin{aligned} \Delta^+(\alpha) &= [\mathbf{u}(\mathbf{x}_0^- + l(\alpha)\mathbf{e}^r(\alpha)) - \mathbf{u}(\mathbf{x}_0^-)] \cdot \mathbf{e}^r(\alpha), \\ \Delta^-(\alpha) &= [\mathbf{u}(\mathbf{x}_0^+) - \mathbf{u}(\mathbf{x}_0^+ - l(\alpha)\mathbf{e}^r(\beta))] \cdot \mathbf{e}^r(\beta). \end{aligned} \tag{43}$$

  Introduction of Eq. (40) into Eq. (42) and using Eqs. (43) and (41), yields

$$\begin{aligned} t_1^+ = &-k\cos\beta\{2u_r^+(\theta)\cos\beta - \cos\alpha[u_r^-(\theta+\gamma) + u_r^-(\theta-\gamma)] \\ &+ \sin\alpha[u_\theta^-(\theta+\gamma) - u_\theta^-(\theta-\gamma)]\}, \\ t_2^+ = &-k\sin\beta\{2u_\theta^+(\theta)\sin\beta + \cos\alpha[u_r^-(\theta+\gamma) - u_r^-(\theta-\gamma)] \\ &- \sin\alpha[u_\theta^-(\theta+\gamma) + u_\theta^-(\theta-\gamma)]\}, \\ t_1^- = &\, k\cos\alpha\{-2u_r^-(\theta)\cos\alpha + \cos\beta[u_r^+(\theta+\gamma) + u_r^+(\theta-\gamma)] \\ &+ \sin\beta[u_\theta^+(\theta+\gamma) - u_\theta^+(\theta-\gamma)]\}, \\ t_2^- = &\, k\sin\alpha\{-2u_\theta^-(\theta)\sin\alpha + \cos\beta[u_r^+(\theta+\gamma) - u_r^+(\theta-\gamma)] \\ &+ \sin\beta[u_\theta^+(\theta+\gamma) + u_\theta^+(\theta-\gamma)]\}. \end{aligned} \tag{44}$$

- To assume that an infinite number of truss elements exist, one at each point of the interface, so that the traction/displacement prescriptions of Eq. (44) hold for

every θ:

$$\sigma_{rr}^{+} = -t_1^{+}, \quad \sigma_{r\theta}^{+} = -t_2^{+}, \quad \sigma_{rr}^{-} = t_1^{-}, \quad \sigma_{r\theta}^{-} = t_2^{-}, \tag{45}$$

where the traction components $t_i^{\pm}$ are given by Eqs. (44). We remark that Eqs. (45) define the interface constitutive law.

It is important to note that the model of a zero-thickness linear interface, connecting a circular inclusion to an infinite matrix, can be obtained from Eqs. (45) by taking $\gamma = c\delta$ (c being a real constant) and letting δ go to zero. In this particular case the angles α and β reduce to the same value, namely

$$\beta_0 = \lim_{\delta \to 0} \left(\arctan \frac{R \sin \gamma}{R + \delta - R \cos \gamma} \right)_{\gamma = c\delta} = \arctan(cR), \tag{46}$$

so that the constitutive Eqs. (45) become

$$[\![\sigma_{rr}]\!] = [\![\sigma_{r\theta}]\!] = 0, \quad \sigma_{rr} = k_r [\![u_r]\!], \quad \sigma_{r\theta} = k_\theta [\![u_\theta]\!], \tag{47}$$

where

$$k_r = \frac{2k}{1 + c^2 R^2}, \quad k_\theta = \frac{2kc^2 R^2}{1 + c^2 R^2}. \tag{48}$$

These equations are identical to those used by a number of authors (see, for instance, Bigoni et al., 1998 and references quoted therein).

4.2. Full-field solution for a circular inclusion with a continuous double Warren truss structural interface

When an infinite matrix connected to a circular inclusion by a continuous double Warren truss structure is loaded by a uniform stress applied at infinity, the stress and displacement fields in both continuous bodies are derived from

$$\begin{aligned} &\phi^{+}(z) = \Gamma_1 z - 2\overline{\Gamma}_2 \frac{B_m}{z}, \quad \psi^{+}(z) = \Gamma_2 z + 4\Gamma_1 \frac{F_m}{z} - 2\overline{\Gamma}_2 \frac{M_m}{z^3}, \\ &\phi^{-}(z) = 4\Gamma_1 A_i z - 2\Gamma_2 B_i z^3, \quad \psi^{-}(z) = -2\Gamma_2 D_i z, \end{aligned} \tag{49}$$

where

$$\Gamma_1 = \frac{\sigma_{11}^{\infty} + \sigma_{22}^{\infty}}{4}, \quad \Gamma_2 = \frac{\sigma_{22}^{\infty} - \sigma_{11}^{\infty}}{2} + \mathrm{i}\sigma_{12}^{\infty}, \tag{50}$$

and the coefficients B_m, F_m, M_m, A_i, B_i, and D_i are determined by imposing the boundary conditions at both sides of the interface, Eqs. $(45)_1$–$(45)_2$ at $r = R + \delta$ and Eqs. $(45)_3$–$(45)_4$ at $r = R$, holding for every θ. The results are

$$\begin{aligned} A_i &= \frac{k(1 + \kappa^{+})(R + \delta)\mu^{-} \cos\beta \cos\alpha}{4[2\mu^{-}\mu^{+} + 2k(R + \delta)\mu^{-}\cos^2\beta + k(\kappa^{-} - 1)R\mu^{+}\cos^2\alpha]}, \\ F_m &= \frac{(R + \delta)^2[-2\mu^{-}\mu^{+} + k(\kappa^{+} - 1)(R + \delta)\mu^{-}\cos^2\beta - k(\kappa^{-} - 1)R\mu^{+}\cos^2\alpha]}{2[2\mu^{-}\mu^{+} + 2k(R + \delta)\mu^{-}\cos^2\beta + k(\kappa^{-} - 1)R\mu^{+}\cos^2\alpha]}, \end{aligned}$$

$$B_i = \frac{\Gamma^{(1)}}{D^{(1)}R^2}\{6\mu^-\mu^+\cos(2\beta+3\gamma) - k[(R+\delta)\mu^-\sin 2\beta\sin 3\gamma + 3R\mu^+\sin\gamma\sin 2\alpha]\},$$

$$\begin{aligned} D_i = & -\frac{6\Gamma^{(1)}\cos\alpha}{D^{(1)}}\{6\mu^-\mu^+\cos(\beta+2\gamma) + k[(R+\delta)\mu^-\sin 2\beta\sin(\beta-2\gamma) \\ & + R\mu^+\sin\alpha(\kappa^-\sin(2\beta+3\gamma) - 3\sin\gamma)]\}, \\ B_m = & \frac{D^{(0)}(R+\delta)^2}{2D^{(1)}}, \end{aligned}$$

$$\begin{aligned} M_m = & B_m(R+\delta)^2 - \frac{\Gamma^{(1)}(R+\delta)^4\mu^+}{D^{(1)}}\{-6\mu^-\cos 2\beta + kR[3\sin(2\beta-\gamma)\sin\gamma \\ & - \kappa^-\sin 3\gamma\sin(2\beta+3\gamma)]\}, \end{aligned} \tag{51}$$

where

$$\begin{aligned} \Gamma^{(i)} = & k(1+\kappa^+)^i(R+\delta)\mu^-, \\ D^{(i)} = & 6(\mu^+)^2\{k^2\kappa^-R^2\sin^2 2\alpha + 2\mu^-[kR(3+\kappa^-) + 6\mu^-]\} + 2^{-i}\Gamma^{(0)}\mu^+ \\ & \times\{-2(-1-3\kappa^+)^i[kR(3+\kappa^-) + 12\mu^-] - 2^ikR[3\cos(4\beta-2\gamma) \\ & + \kappa^-\cos 6\gamma - 3(-\kappa^+)^i(3\cos 2\gamma + \kappa^-\cos(4\beta+6\gamma))]\} - 6(-\kappa^+)^i(\Gamma^{(0)})^2\sin^2 2\beta. \end{aligned} \tag{52}$$

In the limit case of a zero-thickness linear interface, the coefficient $D^{(i)}$ given by Eq. (52) reduces to

$$\begin{aligned} D^{(i)} = & 72(\mu^+\mu^-)^2 + 6k_rk_\theta R^2(\mu^- + \kappa^-\mu^+)[\mu^+ - \mu^-(-\kappa^+)^i] + 6(k_r+k_\theta)R\mu^+\mu^- \\ & \times[(3+\kappa^-)\mu^+ - 2^{1-i}\mu^-(-1-3\kappa^+)^i], \end{aligned} \tag{53}$$

whereas the coefficients given in Eqs. (51) become

$$\begin{aligned} A_i = & \frac{k_r(1+\kappa^+)R\mu^-}{4\{4\mu^-\mu^+ + k_rR[2\mu^- + (\kappa^- - 1)\mu^+]\}}, \\ B_i = & \frac{3R(1+\kappa^+)(k_r-k_\theta)\mu^+(\mu^-)^2}{D^{(1)}R^2}, \\ D_i = & -\frac{3R(1+\kappa^+)k_r\mu^-[6\mu^-\mu^+ + k_\theta R(\mu^- + \kappa^-\mu^+)]}{D^{(1)}}, \end{aligned} \tag{54}$$

$$B_m = \frac{D^{(0)}R^2}{2D^{(1)}}, \quad F_m = \frac{R^2}{2}(4A_i - 1), \quad M_m = R^2(B_m + R^4B_i),$$

which are identical to those found by Bigoni et al. (1998).

4.3. The gradient approximation of a continuous structural interface

In the particular case of an interface comprising fibers characterized by a small angle α, its behavior can be well captured by a gradient approximation of the interface constitutive law. First, we assume that the fiber stiffness k is inversely proportional to

the fibers' length

$$k = \frac{EA}{l(\alpha)}. \tag{55}$$

Thus, the traction transmitted from the interfacial fiber to the elastic body at $\mathbf{x}_j^-$ is a function of the angle α and it can be expanded in Taylor series with remainder about $\alpha = 0$ as

$$\mathbf{t}^-(\alpha) = \sum_{m=0}^{n} \frac{\alpha^m}{m!}\mathbf{t}^{(n)-}(0) + \int_0^\alpha \mathbf{t}^{(n+1)-}(t)\frac{(\alpha - t)^n}{n!}\,\mathrm{d}t, \tag{56}$$

where $\mathbf{t}^{(n)-}$ denotes the nth derivative of $\mathbf{t}^-$ with respect to α.

4.3.1. The zeroth-order approximation

If we retain only the zeroth order terms in Eq. (56), where tractions are given by Eq. (9), we get

$$t_1^- = \frac{EA}{l(0)}[\![\, u_1 \,]\!], \quad t_2^- = 0, \tag{57}$$

where the jump operator is defined as

$$[\![\, \text{quantity} \,]\!] = (\text{quantity at } \mathbf{x}_j^- + l(0)\mathbf{e}_1)_{\Sigma^+} - (\text{quantity at } \mathbf{x}_j^-)_{\Sigma^-}. \tag{58}$$

Note that for a zero-thickness interface, the operator (58) reduces to the usual jump operator defined in Eq. (2). Eqs. (57) give the conditions analyzed by Bigoni and Movchan, [2002; their Eqs. (8) and (9) with $\beta = 0$ or their Eqs. (10) and (11) for the circular geometry with $s_\theta = 0$]; we term this the smeared BM-model. When the thickness of the interface is reduced to zero, Eq. (57) reduces to the usual linear interface constitutive law, but with only normal stiffness.

4.3.2. The first- and second-order approximations: the gradient model

Retaining terms through first order in the Taylor series expansion (56), where tractions are given by Eq. (9), we obtain

$$\begin{aligned} t_1^- &= \frac{EA}{l(0)}[\![\, u_1 \,]\!] + \frac{EA}{l(0)^2}\left[l(0)[\![\, u_2 \,]\!] - l'(0)[\![\, u_1 \,]\!] + l(0)\left(\frac{\partial u_1^+}{\partial \alpha}\right)_{\alpha=0}\right]\alpha, \\ t_2^- &= \frac{EA}{l(0)}[\![\, u_1 \,]\!]\alpha, \end{aligned} \tag{59}$$

where the derivative with respect to α can be evaluated by employing the chain rule as

$$\frac{\partial u_1^+}{\partial \alpha} = \frac{\partial u_1^+}{\partial \mathbf{x}^+} \cdot \frac{\partial \mathbf{x}^+}{\partial \alpha}. \tag{60}$$

Retaining terms through second order in the Taylor series expansion of Eq. (56), we obtain

$$
\begin{aligned}
t_1^- &= \frac{EA}{l(0)}[\![\, u_1 \,]\!] + \frac{EA}{l(0)^2}\left[l(0)[\![\, u_2 \,]\!] - l'(0)[\![\, u_1 \,]\!] + l(0)\left(\frac{\partial u_1^+}{\partial \alpha}\right)_{\alpha=0}\right]\alpha \\
&\quad + \frac{EA}{l(0)}\left[[\![\, u_1 \,]\!]\left(\frac{l'(0)^2}{l(0)^2} - \frac{l''(0)}{2l(0)} - 1\right) - [\![\, u_2 \,]\!]\frac{l'(0)}{l(0)} + \left(\frac{\partial u_2^+}{\partial \alpha}\right)_{\alpha=0}\right. \\
&\quad \left. + \frac{1}{2}\left(\frac{\partial^2 u_1^+}{\partial \alpha^2}\right)_{\alpha=0} - \frac{l'(0)}{l(0)}\left(\frac{\partial u_1^+}{\partial \alpha}\right)_{\alpha=0}\right]\alpha^2, \\
t_2^- &= \frac{EA}{l(0)}[\![\, u_1 \,]\!]\alpha + \frac{EA}{l(0)^2}\left[l(0)[\![\, u_2 \,]\!] - l'(0)[\![\, u_1 \,]\!] + l(0)\left(\frac{\partial u_1^+}{\partial \alpha}\right)_{\alpha=0}\right]\alpha^2.
\end{aligned} \tag{61}
$$

It is evident that Eqs. (59) and (61) contain *gradient terms* related to the geometry of the surfaces joined by the bars. Eqs. (57)–(61) can be employed to develop a continuous model for an interface following the same approach used for the continuous model of Section 4.1.

4.4. Gradient model for a continuous double Warren truss structure—circular inclusion

In the particular case when Σ^+ and Σ^- are two concentric circles with radii R and $R+\delta$ connected by a double Warren truss structure (see Fig. 9) characterized by a small angle α, Eqs. (57)–(61) specialize to

- Zeroth- and first-order approximation

$$
t_1^- = \frac{2EA}{\delta}[\![\, u_r \,]\!], \quad t_1^+ = -t_1^-, \quad t_2^+ = t_2^- = 0. \tag{62}
$$

- Second-order approximation

$$
\begin{aligned}
t_1^+ &= -\frac{2EA}{\delta}[\![\, u_1 \,]\!] - \frac{EA}{\delta}\left[-\frac{R(3R+\delta)}{(R+\delta)^2}[\![\, u_1 \,]\!] + \frac{2R}{R+\delta}\left(\frac{\partial u_2^-}{\partial \alpha}\right)_{\alpha=0} - \left(\frac{\partial^2 u_1^-}{\partial \alpha^2}\right)_{\alpha=0}\right]\alpha^2, \\
t_2^+ &= -\frac{2EAR}{\delta(R+\delta)}\left[\frac{R}{R+\delta}[\![\, u_2 \,]\!] + \left(\frac{\partial u_1^-}{\partial \alpha}\right)_{\alpha=0}\right]\alpha^2, \\
t_1^- &= \frac{2EA}{\delta}[\![\, u_1 \,]\!] + \frac{EA}{\delta}\left[-\frac{3R+2\delta}{R+\delta}[\![\, u_1 \,]\!] + 2\left(\frac{\partial u_2^+}{\partial \alpha}\right)_{\alpha=0} + \left(\frac{\partial^2 u_1^+}{\partial \alpha^2}\right)_{\alpha=0}\right]\alpha^2, \\
t_2^- &= \frac{2EA}{\delta}\left[[\![\, u_2 \,]\!] + \left(\frac{\partial u_1^+}{\partial \alpha}\right)_{\alpha=0}\right]\alpha^2.
\end{aligned} \tag{63}
$$

Note that Eqs. (63) can also be derived directly from Eqs. (44) by expressing the angles β and γ as functions of α, taking into account that

$$
u_1 = u_r\cos\gamma - u_\theta\sin\gamma, \quad u_2 = u_r\sin\gamma + u_\theta\cos\gamma, \tag{64}
$$

and retaining terms through second order in the Taylor series expansion about $\alpha = 0$.

4.5. Full-field solution for a circular inclusion with a gradient–model interface

When a homogeneous stress field is applied at infinity, the analytical solution for a circular inclusion connected to an infinite matrix by a thick interface obeying conditions (63) for every θ and subjected to uniform remote stress (note that condition (62) is a

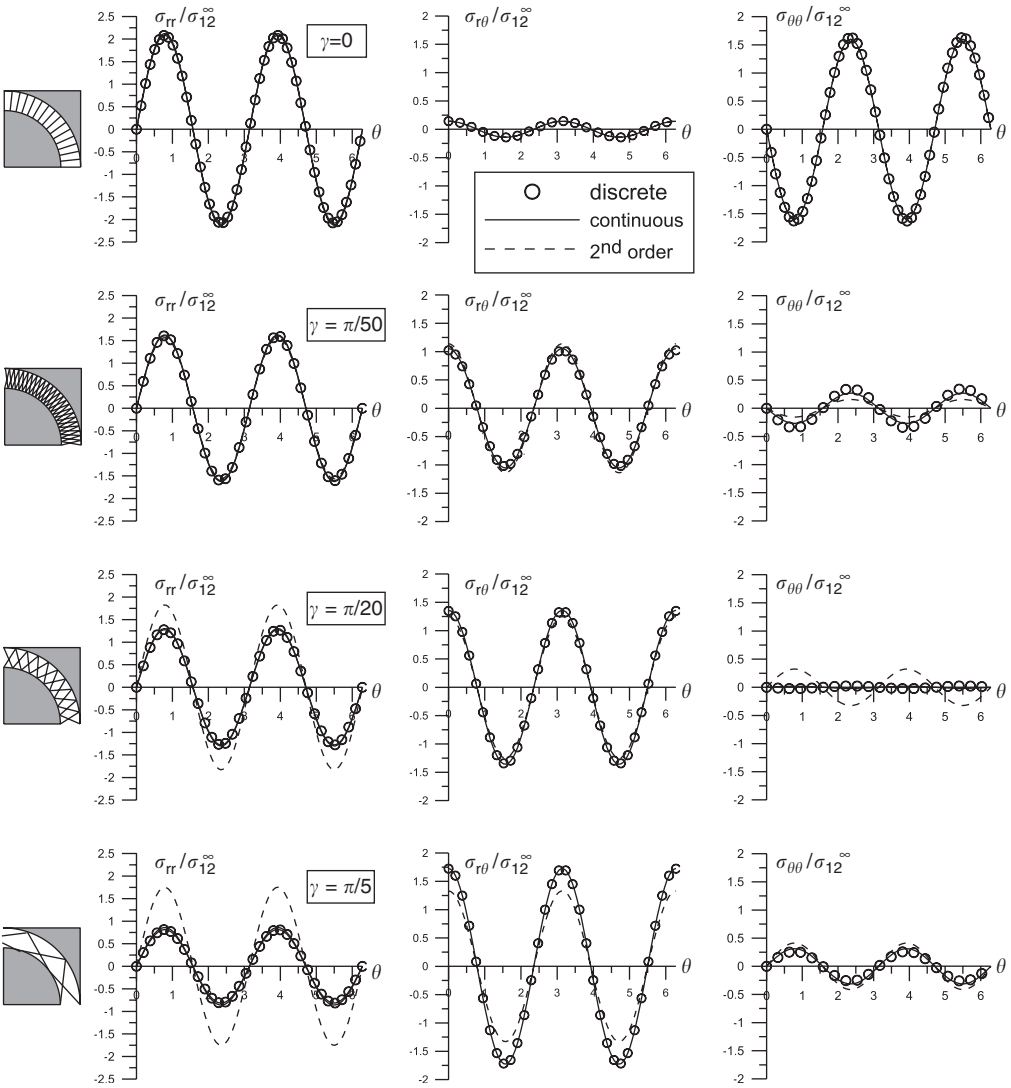

Fig. 10. Stress distribution (in components normalized by the remote stress) at $r = R + 3\delta/2$ in an infinite matrix (with a circular hole of radius $R + \delta$) connected to a circular inclusion (of radius R) by a double Warren truss structure as a function of the angular coordinate θ, for the discrete model with a high bar density (600 truss elements), the continuous model, and its second-order gradient approximation. A remote shear stress σ_{12}^{∞} is applied and different bar inclinations are considered, corresponding to $\gamma = \{0, \pi/50, \pi/20, \pi/5\}$ (see Fig. 9(A)). The inclusion is stiffer than the matrix ($\mu^-/\mu^+ = 10$), $\nu^+ = 0.35$ and $\nu^- = 0.2$, whereas the bars are characterized by $\Lambda_c = 0.077$.

particular case of (63)) is obtained in the same form as given by Eqs. (49). The coefficients in Eqs. (49) can be found by imposing the boundary conditions at both sides of the interface, Eqs. $(63)_1$–$(63)_2$ at $r = R + \delta$ and Eqs. $(63)_3$–$(63)_4$ at $r = R$, holding for every θ. Alternatively, these coefficients can be directly obtained from Eq. (51) by retaining terms through second order in the Taylor series expansion about $\alpha = 0$.

4.6. Continuous versus discrete interface models: comparison of results

We are now in a position to compare full-field solutions for a circular inclusion connected by a double Warren truss structure to an infinite sheet subjected to uniform far

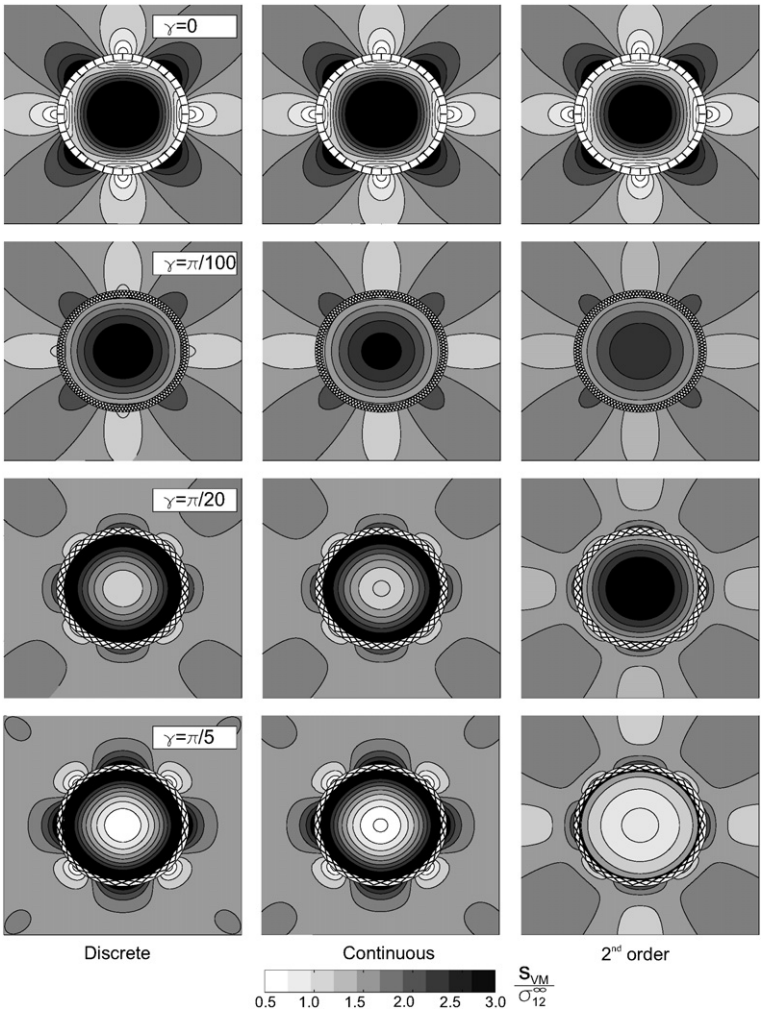

Fig. 11. von Mises stress distribution (normalized by remote stress σ_{12}^{∞}) for a circular inclusion connected to an infinite matrix by a double Warren truss structure and loaded by a remote shear stress for the discrete (with high bar density—600 truss elements, left), continuous (center), and gradient (right) models as a function of the bars' inclination γ, see Fig. 9(A). The inclusion is stiffer than the matrix ($\mu^-/\mu^+ = 10$), $\nu^+ = 0.35$, and $\nu^- = 0.2$, and the bars are characterized by $\Lambda_c = 0.077$.

field loading. The solutions are obtained by using: (i) the analytical discrete-interface approach, (ii) the continuous-interface model, (iii) the interface gradient approximations of various orders. While the first of the three above approaches is completely general, the continuous-interface model and its gradient approximation have been developed for the double Warren truss structure, which reduces to the smeared BM-model and to the zero-thickness linear interface as particular cases. We assume now $\delta = R/10$ and $\mu^-/\mu^+ = 10$, whereas the Poisson ratio for the matrix and the inclusion has been selected—as in Hashin (2002)—equal to $\nu^+ = 0.35$ and $\nu^- = 0.2$. A uniform shear stress $\sigma_{12}^{\infty} = \mu^+/100$ is applied at infinity.

The stress distributions obtained by employing the continuous model and its second-order gradient approximation are compared with that obtained from the discrete model with a large number of bars, namely, 600 truss elements. For the continuous model, the dimensionless compliance parameter

$$\Lambda_c = \frac{2\mu^+}{(\kappa^+ + 1)kR} \tag{65}$$

has been taken as $\Lambda_c = 0.077$, so that in its gradient approximation EA has been chosen equal to $2\mu^+ l/[\Lambda_c R(\kappa^+ + 1)]$, with l denoting the bar length, whereas in the discrete model the bar compliance has been chosen as $\Lambda = \Lambda_c R/t_b$, with $t_b/R = 1/1000$. The stress components (normalized by the remote shear stress) evaluated along a concentric circular path at radius $r = R + 3\delta/2$ in the matrix are plotted in Fig. 10 as a function of the angular coordinate θ. In the graph, continuous lines denote results obtained with the continuous model, dashed lines denote results obtained with its second-order gradient approximation, while symbols denote results of the discrete model. The stress distribution corresponding to the zeroth order approximation is not reported for brevity, since it is coincident with the second-order approximation when $\gamma = 0$, so that *there are no gradient effects*.

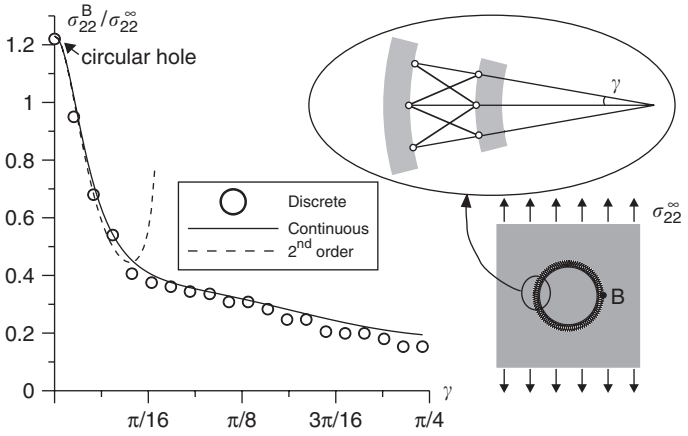

Fig. 12. Stress concentration for a circular inclusion connected to an infinite matrix ($\delta/R = 0.25$) by a discrete (with high bar density—600 truss elements) and a continuous double Warren truss structure, loaded under uniaxial (vertical) stress as a function of the angle γ. The inclusion is stiffer than the matrix ($\mu^-/\mu^+ = 10$), $\nu^+ = \nu^- = \frac{1}{3}$, and the bars are characterized by $\Lambda_c = 0.077$. Note that the second-order gradient approximation also included gives realistic results only for $\gamma < \pi/16$.

In Fig. 11, the level sets of the von Mises stress (normalized by σ_{12}^{∞}) are plotted in a region near the inclusion. Excellent agreement between the discrete and the continuous model is clearly seen from the figure for any angle γ, whereas the second-order gradient model is precise only for small values of γ.

Figs. 10 and 11 show another important feature, namely, that *the gradient effects completely change the stress distribution*. This is evident by comparison of the von Mises stress distribution for $\gamma = 0$ (which, in other words, is a smeared BM-model) with that for $\gamma = \pi/5$.

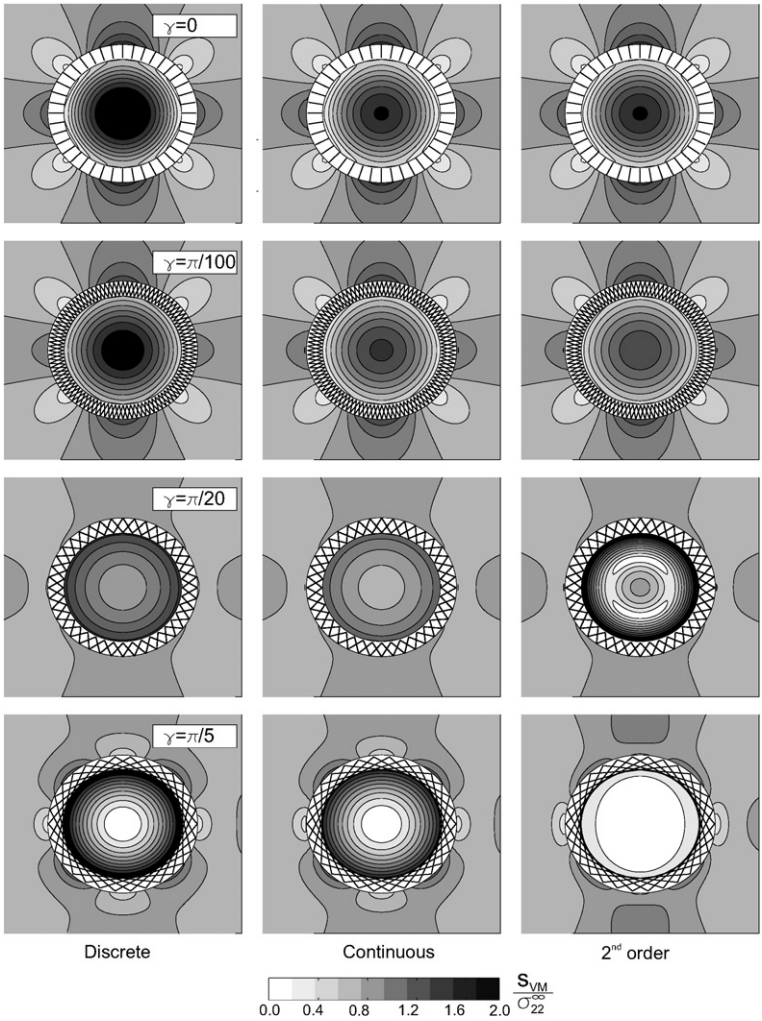

Fig. 13. von Mises stress distribution (normalized by remote stress σ_{22}^{∞}) for a circular inclusion connected to an infinite matrix by a double Warren truss structure and loaded by a uniaxial (vertical) remote stress for the discrete (with high bar density—600 truss elements, left), continuous (center), and gradient (right) models as a function of the bars' inclination γ, see Fig. 9(A). The inclusion is stiffer than the matrix ($\mu^{-}/\mu^{+} = 10$), $v^{+} = v^{-} = \frac{1}{3}$, and the bars are characterized by $\Lambda_c = 0.077$.

Finally, the stress concentration is analyzed at a circular hole of radius $R+\delta$ containing a circular inclusion of radius R so that $\delta/R=0.25$, in an infinite sheet loaded by a uniaxial stress $\sigma_{22}^{\infty}=\mu^{+}/100$ at infinity. Results are reported in Fig. 12 for material properties $\nu^{+}=\nu^{-}=\frac{1}{3}$ and $\mu^{-}/\mu^{+}=10$, and bars characterized by thickness $t_{\mathrm{b}}/R=1/1000$ and compliance $\Lambda_{\mathrm{c}}=0.077$. As in the example above, for the discrete structural interface 600 truss elements have been employed. Cases corresponding to the discrete BM-model (i.e. $\gamma=0$) and the double Warren truss structure are considered together with the continuous model and its second-order gradient approximation. It can be noted that the gradient model gives a good approximation of the stress distribution for γ smaller than $\pi/16$, whereas for larger values of the angle it becomes inaccurate. The stress concentration is strongly influenced by the angle γ (and thus α): increasing the opening of the truss structure causes a larger stress redistribution.

Continuing with this example, the level sets of the von Mises stress for the discrete model, the continuous model, and its second-order gradient approximation are reported in Fig. 13. Also in this case good agreement between the three different models can be observed for γ smaller than $\pi/20$, whereas for $\gamma=\pi/5$ the gradient model is no longer reliable.

In closure, we emphasize that the analytical solution for a circular inclusion connected to an infinite matrix by a *continuous* double Warren structure has been obtained. Furthermore, for a structural interface with bars characterized by a small angle α, the gradient approximation of the constitutive law has been derived, characterized by an analytical representation simpler than that of the continuous model. This is the first example of the analytical derivation of a nonlocal interface model. Finally, we note that a gradient model of the type illustrated here would be especially useful in situations where an exact solution is not possible.

5. Conclusions

In this paper, a novel model of a structural interface capturing the actual physical structure present in the interface has been derived. The model is characterized by a finite thickness and a specific structure, providing a direct description of the relevant microstructure. From the proposed model, nonlocality emerges in a natural, rather than empirical, way, induced directly by the structure joining the two continuous media. The model captures effects absent in all previous interface models including the stress/deformation field effects due to the discrete structure and the great stress concentration reduction due to nonlocality. Starting from the discrete model, a continuum model of a structural interface has been derived. It is interesting to note that the usual zero-thickness linear interface model represents a simple special case of the structural continuum model.

Acknowledgments

Financial support of MURST-Cofin 2003 (prot. 2003082105_002) (K.B. and D.B.) is gratefully acknowledged. Part of this research was performed while D.B. was visiting professor at the Department of Engineering Physics at the University of Wisconsin (Madison, USA), which hospitality is gratefully acknowledged. W.J.D. acknowledges support from Italian Ministry Research Grant 'Rientro dei cervelli MIUR 26/1/2001' and

from Lawrence Livermore National Laboratories under contract W-7405-Eng-48 with the U.S. Department of Energy.

Appendix A. The elastic energies evaluated solving problems (10) and (12) differ by terms of $O(\ell_j^2)$

Taking Taylor series expansions of the displacements and tractions in Eqs. $(10)_2$ and $(10)_3$ about $\ell = 0$, we note the following relationship with the mean values (11)

$$\bar{\mathbf{t}}^j = \mathbf{t}(\mathbf{x}^j) + O(\ell_j^2), \quad \bar{\mathbf{u}}^j = \mathbf{u}(\mathbf{x}^j) + O(\ell_j^2), \tag{A.1}$$

so that, if the junction regions are sufficiently small, a uniform traction corresponds to a uniform displacement, up to $O(\ell_j^2)$. Moreover, let us consider the strain energy of a continuous elastic body connected to other bodies by a structural interface

$$\mathscr{E} = \frac{1}{2}\sum_{j=1}^{N}\int_{\omega_j} \mathbf{t}^j(\mathbf{x})\cdot\mathbf{u}^j(\mathbf{x}) + \frac{1}{2}\int_{\partial\Omega_t}\tilde{\mathbf{t}}\cdot\mathbf{u} + \frac{1}{2}\int_{\partial\Omega_u}\mathbf{t}\cdot\tilde{\mathbf{u}}, \tag{A.2}$$

where $\partial\Omega_t$ and $\partial\Omega_u$ are, respectively, the boundary portions where the tractions $\tilde{\mathbf{t}}$ and the displacements $\tilde{\mathbf{u}}$ are prescribed. Introduction of the Taylor series expansion for $\mathbf{u}$ and $\mathbf{t}$ into the first integral on the right-hand side of Eq. (A.2) yields

$$\frac{1}{2}\sum_{j=1}^{N}\int_{\omega_j}\mathbf{t}^j(\mathbf{x})\cdot\mathbf{u}^j(\mathbf{x}) = \frac{1}{2}\sum_{j=1}^{N}(\bar{\mathbf{t}}^j\cdot\bar{\mathbf{u}}^j)|\omega_j| + O(\ell_j^2). \tag{A.3}$$

Solving problem (12) instead of (10) means that we substitute a general traction distribution within the junction region with a uniform traction $\bar{\mathbf{t}}^j$, so that the discrepancy $\mathbf{t}^*(\mathbf{x})$ with the actual traction distribution $\mathbf{t}(\mathbf{x})$ can be expanded in a Taylor series as

$$\mathbf{t}^*(\mathbf{x}) = \mathbf{t}(\mathbf{x}) - \bar{\mathbf{t}}^j = \frac{\partial\mathbf{t}(\mathbf{x}_j)}{\partial\ell}\ell + O(\ell^2). \tag{A.4}$$

The surface traction $\mathbf{t}^*(\mathbf{x})$ has null resultant force (but possibly nonnull resultant moment) and assume for the moment that the displacement field associated with it is $O(\ell_j^2)$. Therefore, also the tractions induced on $\partial\Omega_u$ by $\mathbf{t}^*(\mathbf{x})$ are $O(\ell_j^2)$. As a conclusion, the energy of the two problems (10) and (12) differs by terms of $\mathrm{O}(\ell_j^2)$.

It remains now to prove that the displacement field associated with $\mathbf{t}^*(\mathbf{x})$ applied on the junctions is $O(\ell_j^2)$. This fact can be inferred from von Mises (1945), Sternberg (1954) and Gurtin (1972). However, von Mises only refers to the behavior in specific cases (a half space and a circular disk) and Sternberg and Gurtin refer to a three-dimensional setting. For completeness, we sketch a nonformal proof of this result for the present two-dimensional framework. The displacement at a boundary point $\mathbf{y} \in \Omega\backslash\bigcup_{j=1}^{N}\omega_j$ is given by the boundary integral equation

$$u_{\mathrm{g}}(\mathbf{y}) = \int_{\omega_j}\tilde{\mathbf{t}}^j(\mathbf{x})\cdot\mathbf{u}^{\mathrm{g}}(\mathbf{x}-\mathbf{y})\,\mathrm{d}\mathbf{x}, \tag{A.5}$$

where $\mathbf{u}^{\mathrm{g}}(\mathbf{x}-\mathbf{y})$ is the Green's function for the solid body Ω. Employing Eq. (A.4) in Eq. (A.5) we get

$$u_{\mathrm{g}}(\mathbf{y}) = \frac{\partial \mathbf{t}(\mathbf{x}_j)}{\partial \ell} \cdot \int_{-\ell_j}^{\ell_j} \mathbf{u}^{\mathrm{g}}(\mathbf{v}(\ell)-\mathbf{y})\ell \,\mathrm{d}\ell, \tag{A.6}$$

which expanded in a Taylor series with respect to the variable ℓ_j becomes

$$u_{\mathrm{g}}(\mathbf{y}) = \frac{2}{3}\frac{\partial \mathbf{u}^{\mathrm{g}}(\mathbf{v}(0)-\mathbf{y})}{\partial \ell}\ell_j^3 = O(\ell_j^2), \tag{A.7}$$

representing the expected result.

Appendix B. Solution for an elliptical inclusion subject to uniform loadings distributed over portions of its boundary

With reference to the problem described in Section 3.1, since the Cartesian components of the outward unit normal to the ellipse $\mathbf{n}$ can be written as

$$n_1 = \frac{\mathrm{d}x_2}{\mathrm{d}s} \quad \text{and} \quad n_2 = -\frac{\mathrm{d}x_1}{\mathrm{d}s}, \tag{B.1}$$

the boundary conditions on the portions of the boundary where tractions are applied can be written as

$$\mathrm{i}(\tilde{t}_1 + \mathrm{i}\tilde{t}_2)\,\mathrm{d}s = (p_k + \mathrm{i}s_k)\,\mathrm{d}z, \tag{B.2}$$

so that

$$F(\sigma) = \begin{cases} 0, & 0<\beta<\beta_1^- \\ \overset{n-1}{\mathrm{T}} + (p_n + \mathrm{i}s_n)\left[R\left(\sigma + \dfrac{m}{\sigma}\right) - z_n^-\right], & \beta_n^- < \beta < \beta_n^+,\ n = 1,\ldots,N \\ \overset{n}{\mathrm{T}}, & \beta_n^+ < \beta < \beta_{n+1}^-,\ n = 1,\ldots,N-1 \\ 0, & \beta_N^+ < \beta < 2\pi, \end{cases} \tag{B.3}$$

where

$$z_k = R(\sigma^k + m\sigma^{-k}),$$
$$\overset{0}{\mathrm{T}} = 0 \quad \text{and} \quad \overset{n}{\mathrm{T}} = \sum_{k=1}^{n}(p_k + \mathrm{i}s_k)(z_k^+ - z_k^-) \quad \text{for } n \neq 0. \tag{B.4}$$

In the limiting case of a concentrated load, since (see Eq. (28))

$$(p_k + \mathrm{i}s_k)(z_k^+ - z_k^-) \to \mathrm{i}(P_k + \mathrm{i}S_k)\mathrm{e}^{\mathrm{i}\theta_k^{\mathbf{n}}}, \tag{B.5}$$

where $\theta_k^{\mathbf{n}}$ denotes the angle between the unit outward normal and the x_1-axis at z_k, Eq. (B.3) reduces to

$$F(\sigma) = \begin{cases} 0, & 0<\beta<\beta_1^- \\ \displaystyle\sum_{k=1}^{n} \mathrm{i}(P_k + \mathrm{i}S_k)\mathrm{e}^{\mathrm{i}\theta_k^{\mathbf{n}}}, & \beta_n < \beta < \beta_{n+1},\ n = 1,\ldots,N-1 \\ 0, & \beta_N < z < 2\pi. \end{cases} \tag{B.6}$$

Since the complex functions $\phi(\zeta)$ and $\psi(\zeta)$ are holomorphic in the circular ring limited by the radii $\rho_{\text{ext}} = 1$ and $\rho_{\text{int}} = \sqrt{m}$, they can be represented as Laurent series

$$\phi(\zeta) = \sum_{k=-\infty}^{+\infty} a_k \zeta^k, \quad \psi(\zeta) = \sum_{k=-\infty}^{+\infty} d_k \zeta^k, \tag{B.7}$$

convergent for $\sqrt{m} < |\zeta| < 1$. Let us consider the conformal mapping of Eq. (16) and two generic points lying on the circle $|\zeta| = \sqrt{m}$, inclined at β and $-\beta$ with respect to the ξ_1-axis. These points correspond to adjacent points on the upper and lower slit faces in the z-plane, so that the continuity conditions

$$\phi(\sqrt{m}\mathrm{e}^{\mathrm{i}\beta}) = \phi(\sqrt{m}\mathrm{e}^{-\mathrm{i}\beta}), \quad \psi(\sqrt{m}\mathrm{e}^{\mathrm{i}\beta}) = \psi(\sqrt{m}\mathrm{e}^{-\mathrm{i}\beta}) \tag{B.8}$$

hold for any β. Substitution of (B.7) into (B.8) gives

$$a_{-k} = m^k a_k, \quad d_{-k} = m^k d_k. \tag{B.9}$$

Since tractions are prescribed on the boundary of the elliptical body in the z-plane, insertion of (B.7) into the complex conjugate of Eq. (22) and multiplication of both sides by ω'/R yields

$$\begin{aligned}(1 - m\mathrm{e}^{-2\mathrm{i}\beta}) \sum_{k=-\infty}^{+\infty} \bar{a}_k \mathrm{e}^{-\mathrm{i}k\beta} + (\mathrm{e}^{-\mathrm{i}\beta} + m\mathrm{e}^{\mathrm{i}\beta}) \sum_{k=-\infty}^{+\infty} k a_k \mathrm{e}^{\mathrm{i}(k-1)\beta} \\ + \sum_{k=-\infty}^{+\infty} b_k \mathrm{e}^{\mathrm{i}k\beta} = \overline{F}(1 - m\mathrm{e}^{-2\mathrm{i}\beta}),\end{aligned} \tag{B.10}$$

where

$$\sum_{k=-\infty}^{+\infty} b_k \zeta^k = \left(1 - \frac{m}{\zeta^2}\right)\psi(\zeta) = \sum_{k=-\infty}^{+\infty} (d_k - m d_{k+2})\zeta^k, \tag{B.11}$$

so that

$$b_k = d_k - m d_{k+2}. \tag{B.12}$$

Since the function F, given in Eq. (B.3), can be expanded in Fourier series as

$$F = \sum_{k=-\infty}^{+\infty} A_k \mathrm{e}^{\mathrm{i}k\beta}, \quad \text{with } A_k = \frac{1}{2\pi}\int_0^{2\pi} F \mathrm{e}^{-\mathrm{i}k\beta}\mathrm{d}\beta, \tag{B.13}$$

yielding

$$\begin{aligned}A_k = \frac{1}{2\pi}\sum_{w=1}^{N}(p_w + \mathrm{i}s_w)\Bigg\{\frac{\mathrm{i}}{k}(z_w^- \mathrm{e}^{-\mathrm{i}k\beta_w^-} - z_w^+ \mathrm{e}^{-\mathrm{i}k\beta_w^+}) + \frac{\mathrm{e}^{-\mathrm{i}k\beta_w^+}}{k^2 - 1}[\mathrm{i}(b + ak)\cos\beta_w^+ \\ -(a + bk)\sin\beta_w^+] - \frac{\mathrm{e}^{-\mathrm{i}k\beta_w^-}}{k^2 - 1}[\mathrm{i}(b + ak)\cos\beta_w^- - (a + bk)\sin\beta_w^-]\Bigg\},\end{aligned} \tag{B.14}$$

the right-hand side of Eq. (B.10) can be rewritten as

$$\overline{F}(1 - m\mathrm{e}^{-2\mathrm{i}\beta}) = \sum_{k=-\infty}^{+\infty} (\bar{A}_{-k} - m\bar{A}_{-k-2})\mathrm{e}^{\mathrm{i}k\beta}. \tag{B.15}$$

Thus, insertion of Eq. (B.15) into Eq. (B.10) and equating terms of equal order yields

$$\bar{a}_{-k} - m\bar{a}_{-k-2} + (k+2)a_{k+2} + mka_k + b_k = \bar{A}_{-k} - m\bar{A}_{-k-2}, \tag{B.16}$$

which, since $\bar{a}_{-k} = m^k \bar{a}_k$ and $\bar{a}_{-k-2} = m^{k+2}\bar{a}_{k+2}$, can be rewritten as

$$\bar{a}_k m^k - \bar{a}_{k+2} m^{k+3} + (k+2)a_{k+2} + mka_k + b_k = \bar{A}_{-k} - m\bar{A}_{-k-2}. \tag{B.17}$$

Putting $k = -k-2$ and observing that

$$b_{-k-2} = d_{-k-2} - md_{-k} = m^{k+2}d_{k+2} - m^{k+1}d_k = -m^{k+1}b_k, \tag{B.18}$$

Eq. (B.16) becomes

$$\bar{a}_{k+2} - m\bar{a}_k - ka_{-k} - m(k+2)a_{-k-2} - m^{k+1}b_k = \bar{A}_{k+2} - m\bar{A}_k. \tag{B.19}$$

It is now possible to eliminate b_k from Eqs. (B.17) and (B.19), obtaining

$$\begin{aligned}&\bar{a}_{k+2}(m^{-k-1} - m^{k+3}) + \bar{a}_k(m^k - m^{-k}) + ka_k(m - m^{-1}) + (k+2)a_{k+2}(1-m^2)\\ &\quad = \bar{A}_{-k} - m\bar{A}_{-k-2} + \frac{\bar{A}_{k+2}}{m^{k+1}} - \frac{\bar{A}_k}{m^k},\end{aligned} \tag{B.20}$$

so that the coefficients a_k can be calculated recursively when a_0 and a_1 are known. From the recursion formula (B.20), we obtain

$$(a_1 + \bar{a}_1)(1-m^2) = \bar{A}_1 - m\bar{A}_{-1}, \tag{B.21}$$

from which $\mathrm{Re}[a_1]$ can be determined, whereas $\mathrm{Im}[a_1]$ remains arbitrary. However, a_0 and $\mathrm{Im}[a_1]$ correspond to a rigid-body motion, so that both are selected equal to zero. In addition, Eq. (B.20) shows that a_2, a_3 and hence all the other even coefficients do not depend on a_0 and $\mathrm{Im}[a_1]$. Defining

$$c_k = ka_k\left(m - \frac{1}{m}\right) + \bar{a}_k\left(m^k - \frac{1}{m^k}\right), \tag{B.22}$$

the recursion formula (B.20) becomes

$$c_k - mc_{k+2} = \bar{A}_{-k} - m\bar{A}_{-k-2} + \frac{\bar{A}_{k+2}}{m^{k+1}} - \frac{\bar{A}_k}{m^k}, \tag{B.23}$$

so that

$$c_k = \bar{A}_{-k} - \frac{\bar{A}_k}{m^k}. \tag{B.24}$$

A closed-form expression for a_k can be found by writing the complex conjugate of Eq. (B.22) and solving for a_k obtaining

$$a_k = \frac{kc_k(m - m^{-1}) - \bar{c}_k(m^k - m^{-k})}{k^2(m-m^{-1})^2 - (m^k - m^{-k})^2}, \quad k > 1, \tag{B.25}$$

these coefficients, together with a_1, render function ϕ known from Eq. $(B.7)_1$.

To complete the solution, namely, to evaluate function ψ, we may determine coefficients b_k from Eq. (B.17) or (B.19) in the form

$$b_k = \bar{A}_{-k} - m\bar{A}_{-k-2} - \bar{a}_k m^k + \bar{a}_{k+2}m^{k+3} - (k+2)a_{k+2} - mka_k. \tag{B.26}$$

Therefore,

$$\left(1-\frac{1}{\zeta^2}\right)\psi(\zeta)=\sum_{k=-\infty}^{+\infty}b_k\zeta^k=\sum_{k=0}^{+\infty}b_k\zeta^k+\sum_{k=1}^{+\infty}b_{-k}\zeta^{-k}, \tag{B.27}$$

is known and, since (from Eq. (B.18)) $b_{-k}=-m^{k-1}b_{k-2}$ and (from Eqs. (B.21) and (B.26)) $b_{-1}=0$, it can be rewritten as

$$\left(1-\frac{1}{\zeta^2}\right)\psi(\zeta)=\sum_{k=0}^{+\infty}b_k\left(\zeta^k-\frac{m^{k+1}}{\zeta^{k+2}}\right), \tag{B.28}$$

which together with Eq. (B.25) represents the solution of the elliptical inclusion problem.

B.1. The particular case of the circular inclusion

The particular case of a circular inclusion of radius R subject to a system of N equilibrated forces is analyzed. Here, the conformal mapping of Eq. (16) reduces to

$$z=R\zeta, \tag{B.29}$$

since $m=0$; therefore, coefficients a_k in Eq. (B.25) simplify to

$$a_k=\begin{cases}0 & \text{if } k<0,\\ A_k & \text{if } k>1,\\ \dfrac{A_1}{2} & \text{if } k=1,\end{cases} \tag{B.30}$$

so that the function ϕ in the ζ-plane becomes

$$\phi(\zeta)=\frac{A_1}{2}\zeta+\sum_{k=2}^{\infty}A_k\zeta^k. \tag{B.31}$$

Substitution of Eq. (B.30) into Eq. (B.26) yields

$$b_k=\begin{cases}0 & \text{if } k<0,\\ \bar{A}_{-k}-(k+2)A_{k+2} & \text{if } k>0,\end{cases} \tag{B.32}$$

so that for the particular case of a circle of radius R the function ψ reduces to

$$\psi(\zeta)=\sum_{k=1}^{\infty}[\bar{A}_{-k}-(k+2)A_{k+2}]\zeta^k. \tag{B.33}$$

For a circular disk of radius R, Eq. (B.14) simplifies to

$$A_k=\frac{\mathrm{i}R}{2\pi k(k-1)}\sum_{w=1}^{N}\{(p_w+\mathrm{i}s_w)[\mathrm{e}^{\mathrm{i}(k\beta_w^-+\beta_w^+)}-\mathrm{e}^{\mathrm{i}(\beta_w^-+k\beta_w^+)}]\}, \tag{B.34}$$

so that Eqs. (B.31) and (B.33) give the solution for a circular disk loaded by an arbitrary number of distributed, uniform loads:

$$\begin{aligned}\phi(\zeta) = & -\frac{R}{4\pi}\sum_{k=1}^{N}(p_k+\mathrm{i}s_k)[\zeta(\beta_k^- - \beta_k^+) + 2\mathrm{i}(\mathrm{e}^{\mathrm{i}\beta_k^-} - \zeta)\log(1-\mathrm{e}^{-\mathrm{i}\beta_k^-}\zeta) \\ & - 2\mathrm{i}(\mathrm{e}^{\mathrm{i}\beta_k^+} - \zeta)\log(1-\mathrm{e}^{-\mathrm{i}\beta_k^+}\zeta)], \\ \psi(\zeta) = & \frac{R}{2\pi\zeta}\sum_{k=1}^{N}\{2s_k\zeta(\mathrm{e}^{-\mathrm{i}\beta_k^-} - \mathrm{e}^{-\mathrm{i}\beta_k^+}) + [2s_k - (\mathrm{i}p_k + s_k)\mathrm{e}^{-\mathrm{i}\beta_k^-}\zeta] \\ & \times \log(1-\mathrm{e}^{-\mathrm{i}\beta_k^-}\zeta) - [2s_k - (\mathrm{i}p_k + s_k)\mathrm{e}^{-\mathrm{i}\beta_k^+}\zeta]\log(1-\mathrm{e}^{-\mathrm{i}\beta_k^+}\zeta)\}. \end{aligned} \tag{B.35}$$

The limiting case of a disk subject to an arbitrary system of concentrated forces can be obtained from Eqs. (B.35) as

$$\begin{aligned}\phi(\zeta) = & -\frac{1}{2\pi}\sum_{k=1}^{N}[(P_k+\mathrm{i}S_k)\mathrm{e}^{\mathrm{i}\beta_k}\log(1-\mathrm{e}^{-\mathrm{i}\beta_k}\zeta)] - \frac{\zeta}{4\pi}\sum_{k=1}^{N}(P_k+\mathrm{i}S_k), \\ \psi(\zeta) = & \frac{1}{2\pi}\sum_{k=1}^{N}[(P_k-\mathrm{i}S_k)\mathrm{e}^{-\mathrm{i}\beta_k}\log(1-\mathrm{e}^{-\mathrm{i}\beta_k}\zeta)] - \frac{1}{2\pi}\sum_{k=1}^{N}\frac{P_k+\mathrm{i}S_k}{\mathrm{e}^{\mathrm{i}\beta_k}-\zeta}, \end{aligned} \tag{B.36}$$

in agreement with Muskhelishvili (1953).

Appendix C. Solution for an elliptical hole in an infinite matrix subject to uniform loadings distributed over portions of the hole boundary

To solve the problem described in Section 3.2, the conformal mapping (Eq. (16)) is substituted into the boundary conditions (Eq. (22)), yielding

$$\phi(\sigma) + \frac{\sigma^2+m}{\sigma(1-m\sigma^2)}\overline{\phi'(\sigma)} + \overline{\psi(\sigma)} = F(\sigma), \tag{C.1}$$

or in complex conjugate form

$$\overline{\phi(\sigma)} + \frac{\sigma(1+m\sigma^2)}{\sigma^2-m}\phi'(\sigma) + \psi(\sigma) = \overline{F(\sigma)}. \tag{C.2}$$

Since the resultant of the applied external loads is zero (this load will be transmitted by the structural interface at the contacts) and the stress vanishes at infinity, $\phi(\zeta)$ and $\psi(\zeta)$ are holomorphic for $|\zeta|>1$, including the point at infinity. Therefore, Cauchy's formula for the infinite region can be employed,

$$\frac{1}{2\pi\mathrm{i}}\int_{|\zeta|=1}\phi(\sigma)\frac{\mathrm{d}\sigma}{\sigma-\zeta} = -\phi(\zeta), \tag{C.3}$$

so that multiplication of Eqs. (C.1) and (C.2) by $1/[2\pi\mathrm{i}(\sigma-\zeta)]$ and integration over the contour yields

$$\phi(\zeta) = -\frac{1}{2\pi\mathrm{i}}\int_{|\zeta|=1}\frac{F(\sigma)}{\sigma-\zeta}\,\mathrm{d}\sigma, \tag{C.4}$$

and

$$\psi(\zeta) = -\frac{1}{2\pi \mathrm{i}} \int_{|\zeta|=1} \frac{\overline{F(\sigma)}}{\sigma - \zeta} \, \mathrm{d}\sigma - \zeta \frac{1 + m\zeta^2}{\zeta^2 - m} \phi'(\zeta). \tag{C.5}$$

The Eqs. (C.4) and (C.5) have been obtained by taking into account that

$$\frac{1}{2\pi \mathrm{i}} \int_{|\zeta|=1} \frac{\overline{\phi(\sigma)}}{\sigma - \zeta} \, \mathrm{d}\sigma = 0,$$

and

$$\frac{1}{2\pi \mathrm{i}} \int_{|\zeta|=1} \sigma \frac{1 + m\sigma^2}{\sigma^2 - m} \frac{\phi'(\sigma)}{\sigma - \zeta} \, \mathrm{d}\sigma = -\zeta \frac{1 + m\zeta^2}{\zeta^2 - m} \phi'(\zeta).$$

When N constant tangential and normal loads p_k and s_k are applied at the boundary of the elliptical hole, the function $F(\sigma)$ in Eq. (C.1) is obtained in the same way as for the elliptical inclusion, yielding again Eq. (B.3). Introducing Eq. (B.3) into (C.4) and (C.5) and using the facts that

$$\int_{\sigma_k^-}^{\sigma_k^+} \frac{\mathrm{d}\sigma}{\sigma - \zeta} = \log\left(\frac{\sigma_k^+ - \zeta}{\sigma_k^- - \zeta}\right), \tag{C.6}$$

$$\int_{\sigma_k^-}^{\sigma_k^+} \left(\sigma + \frac{m}{\sigma}\right) \frac{\mathrm{d}\sigma}{\sigma - \zeta} = \sigma_k^+ - \sigma_k^- - \frac{m}{\zeta} \log \frac{\sigma_k^+}{\sigma_k^-} + \left(\zeta + \frac{m}{\zeta}\right) \log\left(\frac{\sigma_k^+ - \zeta}{\sigma_k^- - \zeta}\right), \tag{C.7}$$

$$\int_{\sigma_k^-}^{\sigma_k^+} \left(m\sigma + \frac{1}{\sigma}\right) \frac{\mathrm{d}\sigma}{\sigma - \zeta} = m\sigma_k^+ - m\sigma_k^- - \frac{1}{\zeta} \log \frac{\sigma_k^+}{\sigma_k^-} + \left(m\zeta + \frac{1}{\zeta}\right) \log\left(\frac{\sigma_k^+ - \zeta}{\sigma_k^- - \zeta}\right), \tag{C.8}$$

and the resultant applied force is zero, i.e.

$$\sum_{k=1}^{N} (p_k + \mathrm{i}s_k)(z_k^+ - z_k^-) = 0, \tag{C.9}$$

we finally obtain the solution for an elliptical hole in an elastic matrix loaded by piecewise constant normal and tangential tractions:

$$\begin{aligned}
\phi(\zeta) = & -\frac{1}{2\pi \mathrm{i}} \sum_{k=1}^{N} (p_k + \mathrm{i}s_k) \left\{ R\left[\sigma_k^+ - \sigma_k^- - \frac{m}{\zeta} \log \frac{\sigma_k^+}{\sigma_k^-} + \left(\zeta + \frac{m}{\zeta}\right) \log\left(\frac{\sigma_k^+ - \zeta}{\sigma_k^- - \zeta}\right)\right] \right. \\
& \left. + z_k^- \log(\sigma_k^- - \zeta) - z_k^+ \log(\sigma_k^+ - \zeta) \right\}. \\
\psi(\zeta) = & -\frac{1}{2\pi \mathrm{i}} \sum_{k=1}^{N} (p_k - \mathrm{i}s_k) \left\{ R\left[m\sigma_k^+ - m\sigma_k^- - \frac{1}{\zeta} \log \frac{\sigma_k^+}{\sigma_k^-} + \left(m\zeta + \frac{1}{\zeta}\right) \log\left(\frac{\sigma_k^+ - \zeta}{\sigma_k^- - \zeta}\right)\right] \right. \\
& \left. + \overline{z}_k^- \log(\sigma_k^- - \zeta) - \overline{z}_k^+ \log(\sigma_k^+ - \zeta) \right\} - \frac{\zeta(1 + m\zeta^2)}{\zeta^2 - m} \phi'(\zeta),
\end{aligned} \tag{C.10}$$

where $\phi'(\zeta)$ is the first derivative of ϕ with respect to ζ. In Eqs. (C.10), the term $\log \sigma_k^+/\sigma_k^-$ corresponds to $i\Theta$, with Θ being the angular distance between the points from σ_k^- to σ_k^+, measured counter-clockwise.

References

Argatov, I.I., Nazarov, S.A., 1994. Asymptotic solution to the problem of an elastic body lying on several small supports. J. Appl. Math. Mech. 58, 303–311.

Benveniste, Y., Miloh, T., 2001. Imperfect soft and stiff interfaces in two-dimensional elasticity. Mech. Mater. 33, 309–323.

Bigoni, D., Movchan, A.B., 2002. Statics and dynamics of structural interfaces in elasticity. Int. J. Solids Struct. 39, 4843–4865.

Bigoni, D., Serkov, S.K., Valentini, M., Movchan, A.B., 1998. Asymptotic models of dilute composites with imperfectly bonded inclusions. Int. J. Solids Struct. 35, 3239–3258.

Camacho, G.T., Ortiz, M., 1996. Computational modelling of impact damage in brittle materials. Int. J. Solids Struct. 33, 2899–2938.

Ciarlet, P.G., 1990. Plates and Junctions in Elastic Multi-Structures. Masson, Paris.

Ciarlet, P.G., 1997. Mathematical Theory of Elasticity. Vol. II: Theory of Plates. North-Holland, Amsterdam.

Ciarlet, P.G., Le Dret, H., Nzengwa, R., 1989. Junctions between 3D and 2D linear elastic structures. J. Math. Pures Appl. 68, 261–295.

Conca, C., Zuazua, E., 1994. Asymptotic analysis of a multidimensional vibrating structure. SIAM J. Math. Anal. 25, 836–858.

Esposito, L., Sciti, D., Piancastelli, A., Bellosi, A., 2004. Microstructure and properties of porous β-SiC templates from soft woods. J. Eur. Ceram. Soc. 24, 533–540.

Gao, H.J., Huang, Y.G., Abraham, F.F., 2001. Continuum and atomistic studies of intersonic crack propagation. J. Mech. Phys. Solids 49, 2113–2132.

Geers, M.G.D., 1997. Experimental analysis and computational modelling of damage and fracture. Ph.D. Thesis, Technische Universitet Eindhoven.

Gei, M., Genna, F., Bigoni, D., 2002. An interface model for the periodontal ligament. J. Biomech. Eng. ASME 124, 538–546.

Gibson, L.J., Ashby, M.F., Karam, G.N., Wegst, U., Shercliff, H.R., 1995. The mechanical properties of natural materials. II. Microstructures for mechanical efficiency. Proc. Math. Phys. Sci. 450, 141–162.

Gurtin, M.E., 1972. The linear theory of elasticity. In: Flügge, S. (Ed.), Encyclopedia of Physics, vol. VIa/2. Springer, Berlin, pp. 1–295.

Hashin, Z., 2002. Thin interphase/imperfect interface in elasticity with application to coated fiber composites. J. Mech. Phys. Solids 50, 2509–2537.

Jackson, A.P., Vincent, J.F.V., Turner, R.M., 1988. The mechanical design of nacre. Proc. R. Soc. London Series B – Biol. Sci. 234, 415–440.

Kahle, W., Frotscher, M., 2002. Nervous System and Sensory Organs. G. Thieme Verlag, Stuttgart.

Kozlov, V.A., Maz'ya, V.G., Movchan, A.B., 1999. Asymptotic Analysis of Fields in Multi-Structures. Oxford University Press, Oxford.

Kozlov, V.A., Maz'ya, V.G., Movchan, A.B., 2001. Fields in non-degenerate 1D–3D elastic multi-structures. Q. J. Mech. Appl. Math. 34, 177–212.

Levy, A.J., Dong, Z.F., 1998. Effective transverse response of fiber composites with nonlinear interface. J. Mech. Phys. Solids 46, 1279–1300.

Levy, A.J., Hardikar, K., 1999. The inclusion pair interaction problem with non-linear interface. J. Mech. Phys. Solids 47, 1477–1508.

Lipton, R., Talbot, D.R.S., 2001. Bounds for the effective conductivity of a composite with an imperfect interface. Proc. R. Soc. London 457, 1501–1517.

Mann, K.A., Werner, F.W., Ayers, D.C., 1997. Modeling the tensile behavior of the cement–bone interface using nonlinear fracture mechanics. J. Biomech. Eng. ASME 119, 175–178.

Mises, R.v., 1945. On Saint Venant's principle. Bull. Am. Math. Soc. 51, 555–562.

Movchan, A.B., Bullough, R., Willis, J.R., 2003. Two-dimensional lattice models of the Peierls type. Philos. Mag. 83, 569–587.

Muskhelishvili, N.I., 1953. Some Basic Problems of the Mathematical Theory of Elasticity. Noordhoff, Groningen, Holland.
Needleman, A., 1992. Micromechanical modeling of interfacial decohesion. Ultramicroscopy 40, 203–214.
Puel, J.P., Zuazua, E., 1993. Exact controllability for a model of a multidimensional flexible structure. Proc. R. Soc. Edinburgh 123A, 323–344.
Radi, E., Bigoni, D., Tralli, A., 1999. On uniqueness for frictional contact rate problems. J. Mech. Phys. Solids 47, 275–296.
Rice, J.R., Wang, J.S., 1989. Embrittlement of interfaces by solute segregation. Mater. Sci. Eng. A 107, 23–40.
Rubin, M.B., Benveniste, Y., 2004. A Cosserat shell model for interphases in elastic media. J. Mech. Phys. Solids 52, 1023–1052.
Rubinstein, A.A., 1994. Strength of fiber reinforced ceramics on the basis of a micromechanical analysis. J. Mech. Phys. Solids 42, 401–422.
Sternberg, E., 1954. On Saint Venant's principle. Q. Appl. Math. 11, 393–402.
Xiao, F., Curtin, W.A., 1995. Numerical investigation of polymer craze growth and fracture. Macromolecules 28, 1654–1660.